THE ASTROPHYSICAL JOURNAL, 412:593–611, 1993 August 1

COLLISIONS AND CLOSE ENCOUNTERS BETWEEN MASSIVE MAIN-SEQUENCE STARS

DONG LAI,[1] FREDERIC A. RASIO,[2,3] AND STUART L. SHAPIRO[1,4]
Center for Radiophysics and Space Research, Cornell University, Ithaca, NY 14853
Received 1992 November 18; accepted 1993 February 9

ABSTRACT

Collisons and close encounters between two massive ($1 \lesssim M/M_\odot \lesssim 100$) main-sequence stars have been studied using smooth-particle hydrodynamics (SPH). The stars are represented by Eddington standard models, which have the density profile of a polytrope with $n = 3$ but mass-dependent binding energy and adiabatic index $4/3 < \Gamma_1 < 5/3$. The equation of state is that of an ideal gas plus thermal radiation. We have performed a large number of calculations to obtain extensive coverage of the parameter space. In particular, the stellar masses, relative velocity, and collision impact parameter are all varied over wide ranges, representative of the conditions encountered in dense stellar systems such as galactic nuclei. We give approximate scaling relations and fitting formulae for the amount of mass loss and for the critical impact parameters for capture or merging. The more massive stars, which have smaller ratios of specific binding energy to the square of escape velocity, are more easily disrupted in collisions. In the limit of small relative velocity, our results for the tidal capture radius agree closely with those of linear perturbation theory, although some nonlinear effects are always apparent. As the relative velocity increases, the orbital energy of the colliding stars can only be dissipated by shock heating, and the critical capture radius decreases much faster than predicted by linear theory. We also calculate cross sections and rates of stellar capture, merging, and mass loss in a dense star cluster. We find that the average fractional mass loss per collision in a cluster does not depend sensitively on the stellar velocity dispersion. Even when the velocity dispersion is as large as several times the typical escape velocity from a star, collisions are not very disruptive on the average, with only a few percent of the mass liberated per collision. Our results should be useful for future dynamical studies of dense stellar systems incorporating the effects of stellar collisions and close dissipative encounters.

Subject headings: celestial mechanics, stellar dynamics — galaxies: nuclei — globular clusters: general — hydrodynamics — stars: interiors — stars: mass loss

1. INTRODUCTION AND MOTIVATION

Stellar densities and velocity dispersions in dense systems such as galactic nuclei can reach values such that close stellar encounters and physical collisions play an important role in their dynamical evolution. There is now direct observational evidence for the existence of star clusters with densities $\rho \sim 10^6$–$10^9\ M_\odot\ \mathrm{pc}^{-3}$ and three-dimensional velocity dispersions $\sigma \sim 10^2$–$10^3\ \mathrm{km\ s}^{-1}$ in the nuclei of nearby galaxies. For example, recent *HST* Planetary Camera images of M32 have revealed a dense, unresolved nucleus with density $\rho > 4 \times 10^6\ M_\odot\ \mathrm{pc}^{-3}$ and velocity dispersion $\sigma > 100\ \mathrm{km\ s}^{-1}$ (Lauer et al. 1993). In M31, the central velocity dispersion $\sigma \simeq 380\ \mathrm{km\ s}^{-1}$, and the density $\rho \gtrsim 10^7\ M_\odot\ \mathrm{pc}^{-3}$ (Dressler & Richstone 1988; Kormendy 1988). In M87, the central velocity dispersion is even higher, $\sigma > 600\ \mathrm{km\ s}^{-1}$, comparable to the escape velocity from the surface of a main-sequence star, and the mass within the central few parsecs is greater than $10^9\ M_\odot$ (Dressler 1989; Lauer et al. 1992). These recent observations of galactic nuclei also indicate the likely presence of a massive black hole at the center (see Dressler 1989 and Kormendy 1993 for reviews). Theorists have suggested in fact that most galaxies probably contain a central massive black hole (Rees 1990). If this is the case, then the stellar density and velocity dispersion are even higher near the black hole, and physical collisions between stars are inevitably important. Main-sequence (MS) stars with a wide range of masses are likely to be involved in these collisions.

In the cores of globular clusters, although the density $\rho \lesssim 10^6\ M_\odot\ \mathrm{pc}^{-1}$ and velocity dispersion $\sigma \sim 10$–$50\ \mathrm{km\ s}^{-1}$ are typically smaller than in galactic nuclei, close stellar encounters may also be dynamically important (see, e.g., Spitzer 1987, chap. 6). In addition, they are expected to produce a variety of interesting observable objects at rates far exceeding those in the rest of the Galaxy. In particular, low-mass X-ray binaries and millisecond pulsars are thought to result from close encounters between a MS or red-giant star and a neutron star (Davies, Benz, & Hills 1992; Di Stefano & Rappaport 1992; Rasio & Shapiro 1991). Collisions between two MS stars could be responsible for the formation of blue stragglers (Hills & Day 1976; Leonard 1989), which are now being discovered in large numbers in the cores of dense clusters (Paresce et al. 1991, 1993; Guhathakurta et al. 1993). Collision rates in globular clusters can be increased considerably by the presence of even a small population of primordial binaries, for which there is now clear observational evidence (see Hut et al. 1992 for a recent review).

In all dense stellar systems, two-body relaxation drives secular core collapse, which causes the central velocity dispersion and stellar density to rise. Consequently, stellar collisions will inevitably become important for the final dynamical evolution of these systems. Collisions and close encounters between stars can affect the dynamical evolution of a stellar cluster in several distinct ways. When the local velocity dispersion exceeds the typical escape velocity from the surface of a star ($\simeq 600\ \mathrm{km\ s}^{-1}$ for a solar-type MS star), the time between

[1] Department of Physics, Cornell University.
[2] Hubble Fellow.
[3] Postal address: Institute for Advanced Study, Princeton, NJ 08540.
[4] Department of Astronomy, Cornell University.

collisions can be shorter than the relaxation time and the dynamical evolution is drastically affected (see, e.g., Binney & Tremaine 1987, chap. 8). But even when the velocity dispersion is smaller than the escape velocity, collisions can lead to dissipation of the kinetic energy of the cluster (when a merger results), or can provide an energy source to the cluster (when a binary forms in a dissipative encounter). In addition, massive stars formed from mergers tend to speed up the evolution of the cluster following mass segregation. Collisions are also very important in star clusters containing a central massive black hole. In particular, they are expected to drive the cusp density profile away from the familiar $r^{-7/4}$ power law appropriate for point masses (Bahcall & Wolf 1976; Frank & Rees 1976; Lightman & Shapiro 1976; see Shapiro 1985 for a recent review). The gaseous debris liberated from stellar collisions could also provide fuel for accretion onto massive black holes in quasars and other active galactic nuclei.

Early studies of stellar collisions in galactic nuclei focused on trying to explain the luminosity of quasars as arising from disruptive stellar collisions (Gold, Axford, & Ray 1965; Spitzer & Saslaw 1966; Spitzer & Stone 1967) or from supernovae triggered by the rapid build-up of massive stars in successive collisions (Colgate 1967). While it is now accepted that stellar collisions are probably not the energy source of active galactic nuclei, they could provide an important route for the formation of supermassive black holes in these systems (Begelman & Rees 1978; Rees 1984). Indeed, highly disruptive stellar collisions between massive stars could dissolve the stellar core into a gas cloud, which eventually collapses to a black hole. Alternatively, stellar collisions and mergers could lead to the runaway formation of a central supermassive star or the production of a cluster of neutron stars and stellar-mass black holes, which ultimately can collapse to a massive black hole (Zel'dovich & Podurets 1965; Rees 1984; Shapiro & Teukolsky 1985; Quinlan & Shapiro 1989).

Recently, Fokker-Planck simulations of the dynamical evolution of galactic nuclei have been performed (David, Durisen, & Cohn 1987a, b; Quinlan & Shapiro 1990; Murphy, Cohn, & Durisen 1991). The results of these studies depend sensitively on their treatment of stellar collisions. So far, however, all treatments were based on rather crude approximate models similar to those introduced in the pioneering works by Spitzer & Saslaw (1966; see also Murphy et al. 1991) and Sanders (1970). In these models, the outcome of a collision is determined on the basis of very simple "rules" obtained from energy and momentum conservation. Important hydrodynamic effects, such as shock propagation, are neglected entirely, and a simple one-dimensional geometry is adopted. Clearly, a reexamination of the effects of stellar collisions in galactic nuclei, based on state-of-the-art hydrodynamic calculations in three dimensions, appears highly desirable.

Early hydrodynamic calculations of stellar collisions were restricted to the axisymmetric, head-on case (Mathis 1967; DeYoung 1968; Seidl & Cameron 1972), with further simplifying approximations often necessary. It is only recently that fully three-dimensional calculations have become possible, using either the smooth particle hydrodynamics (SPH) method (Benz & Hills 1987, 1992; Cleary & Monaghan 1990; Davies et al. 1992; Goodman & Hernquist 1991; Rasio & Shapiro 1991) or more traditional finite-difference methods such as PPM (Ruffert & Müller 1990; Ruffert 1992). All of these studies have focused on globular clusters, where the stars involved are low-mass ($M \lesssim 0.8\ M_\odot$) MS stars or red giants and the impact velocities are nearly parabolic. In the simulations of main-sequence star collisions by Benze & Hills (1987, 1992), the colliding stars were modeled as $n = 3/2$ polytropes with adiabatic index $\Gamma_1 = 5/3$. This model is only appropriate for very low-mass stars with convective envelopes ($M \lesssim 0.4\ M_\odot$). For higher mass MS stars with radiative envelopes ($M \gtrsim 1\ M_\odot$), the density profile is closer to that of an $n = 3$ polytrope. Moreover, radiation pressure can become important in the equation of state, so that the adiabatic index Γ_1 is between 4/3 and 5/3.

In contrast to globular clusters, galactic nuclei may very well contain younger, more massive MS stars with hyperbolic relative velocities. In addition, because of their higher stellar density and velocity dispersion, successive stellar collisions and mergers will likely result in the buildup of very massive stars (Colgate 1967; Sanders 1970; Quinlan & Shapiro 1990). Although globular clusters consist mainly of low-mass MS stars, more massive stars could also form in their cores by the process of successive mergers. These could result from single stars going through successive collisions, or from the resonant interaction between binaries (Goodman & Hernquist 1991). The recent observation that about 15% of blue stragglers in globular clusters may have masses above twice the turn-off mass (Sarajedini 1993) provides some evidence that these processes might indeed occur. Close encounters between massive MS stars could also be important for the dynamical evolution of young open clusters (Pols 1993), and could play a role during the formation of stellar groups and associations. Much denser clusters containing young massive stars have also been observed recently in the Large Magellanic Cloud (see Meylan 1993).

In this paper we use the SPH method to calculate collisions and close encounters between high-mass MS stars. We model the stars as Eddington standard models (i.e., constant ratio of radiation pressure to gas pressure throughout the star; see § 2). This model is appropriate for MS stars with masses in the range $1\ M_\odot \lesssim M \lesssim 100\ M_\odot$. Our goal is to obtain a thorough understanding of the physics of stellar collisions and close dissipative encounters for MS stars in this mass range. In particular, we seek to answer two questions: (1) Given the stellar masses, relative velocity, and impact parameter of the colliding stars, what is the qualitative outcome of an encounter? (2) How much mass is lost in the process?

Our paper is organized as follows. In § 2, we discuss some qualitative features of our stellar model and the collision processes, and derive some simple approximate scaling relations. In § 3, we discuss our numerical method, including the set-up of the initial conditions, mass-loss criterion, and the determination of the critical capture radius. In § 4, we present our numerical results, including fitting formulae for important quantities. In § 5, we apply our results to typical star clusters, obtaining cross sections and rates for various processes. In § 6 we briefly summarize our findings.

2. QUALITATIVE OVERVIEW OF STELLAR COLLISIONS

In this section we introduce our model of a MS star, define the key physical parameters, and derive some approximate scaling relations. We also discuss qualitatively the various possible outcomes of close stellar encounters.

We specify a given stellar encounter by four parameters: the masses of the two stars M_1 and M_2 (or, the mass of the more massive star M_1 and the mass ratio $q = M_2/M_1 \leq 1$), the relative velocity at infinity v_∞, and the periastron distance r_p

(corresponding to the trajectory that the two stars would flow if they were point masses). We determine the stellar radii from the approximate mass-radius relation $R \propto M^{0.8}$. More realistic mass-radius relations for MS stars take the form $R \propto M^{\delta}$, with $\delta \simeq 0.5$–0.8, but our results are not very sensitive to the particular choice of exponent.

2.1. *The Eddington Standard Model*

The Eddington standard model of a MS star (see, e.g., Clayton 1983) is characterized by a constant ratio β of gas pressure to total pressure throughout the star, so that

$$P_{\rm gas} = \frac{\rho k T}{\mu_m m_p} \equiv \beta P ,$$

$$P_{\rm rad} = \frac{1}{3} a T^4 \equiv (1-\beta) P , \tag{2.1}$$

where μ_m is the mean molecular weight, m_p is the proton mass, a is the radiation constant and k is Boltzmann's constant. The pressure-to-density relation that determines the density profile of the star in hydrostatic equilibrium is then

$$P = K(\beta)\rho^{4/3} , \tag{2.2a}$$

with

$$K(\beta) = \left[\left(\frac{k}{\mu_m m_p}\right)^4 \frac{3(1-\beta)}{a\beta^4}\right]^{1/3} . \tag{2.2b}$$

Therefore the density profile is that of a $n = 3$ polytrope. It is convenient to define a nondimensional "mass parameter" α via

$$\alpha \equiv \mu_m^2 \frac{M}{M_c} , \tag{2.3a}$$

where M_c is given by a combination of fundamental constants according to

$$M_c \equiv \frac{k^2}{m_p^2 G^{3/2} a^{1/2}} = \left(\frac{\pi^2}{15}\right)^{-1/2} (\alpha_G^{-3/2} m_p) = 2.28\ M_\odot . \tag{2.3b}$$

Here $\alpha_G = Gm_p^2/\hbar c$ is the dimensionless gravitational "fine structure" constant and $\alpha_G^{-3/2} m_p = 1.85\ M_\odot$. For a given mass parameter α, the value of β is uniquely determined by the equation

$$7.89 \frac{(1-\beta)^{1/2}}{\beta^2} = \alpha . \tag{2.4}$$

Thus radiation pressure is important only for very massive stars ($\alpha \gtrsim 10$, i.e., $M/M_\odot \gtrsim 50$ for $\mu_m \simeq 0.6$). Using the virial relation, the total energy of a star of mass M and radius R is given by

$$E = \frac{1}{2}\beta W = -\frac{3}{4}\beta \frac{GM^2}{R} , \tag{2.5}$$

where W is the gravitational potential energy.

Although the density profile of the standard model is that of a $n = 3$ polytrope, the adiabatic index Γ_1 governing perturbations is given by

$$\Gamma_1 \equiv \left(\frac{\partial P}{\partial \rho}\right)_S = \frac{32 - 24\beta - 3\beta^2}{24 - 21\beta} , \tag{2.6}$$

(see, e.g., Clayton 1983). Hence in general, $4/3 < \Gamma_1 < 5/3$. For high-mass stars $\beta \ll 1$ and $\Gamma_1 \simeq 4/3$, while for low-mass stars, $\beta \simeq 1$ and $\Gamma_1 \simeq 5/3$. The adiabatic index $\Gamma = 1 + 1/n$ governing the polytropic equilibrium density profile ($P \propto \rho^{\Gamma}$), is 4/3 in all cases.

2.2. *Disruption Velocity and Mass Loss*

When two identical stars collide head-on, the minimum relative velocity at infinity v_d required for compete disruption is given approximately by the condition that the total energy in the center of mass frame be zero,

$$\frac{M}{4} v_d^2 = 2|E| = \frac{3}{2}\beta \frac{GM^2}{R} . \tag{2.7}$$

This condition gives

$$v_d = (6\beta)^{1/2}\left(\frac{GM}{R}\right)^{1/2} = (3\beta)^{1/2} v_{\rm esc}$$

$$\simeq 1070\beta^{1/2}\left(\frac{M}{M_\odot}\right)^{1/2}\left(\frac{R}{R_\odot}\right)^{-1/2} \text{km s}^{-1} , \tag{2.8}$$

where $v_{\rm esc}$ is the escape velocity from one star. Clearly, high-mass stars (which have small β) have smaller ratios of v_d to $v_{\rm esc}$ and hence can be disrupted more easily than lower mass stars.

For collisions between stars of different masses, the disruption velocity v_d is higher since for a given relative velocity, less kinetic energy is available in the center-of-mass frame to disrupt the stars. In addition, because of the difference in the stellar radii, a smaller fraction of the stellar volume participates in the impact. Therefore, when the mass ratio is small, the stars can avoid disruption even at very high impact velocity. This expectation is confirmed by our numerical results (see § 4).

Since the more massive star has a smaller specific binding energy and a lower density ($\bar{\rho} \propto M/R^3 \propto M^{-1.4}$ for $R \propto M^{0.8}$), most of the material lost in a collision comes from the more massive star (M_1). The ejected material must carry away energy per unit mass $\sim \beta_1 GM_1/R_1$, corresponding to the specific binding energy of the more massive star. For two stars colliding with relative velocity at infinity $v_\infty \gg v_{\rm esc}$, the available kinetic energy is $\sim \mu v_\infty^2$, where μ is the reduced mass. Therefore, the mass fraction that can be lost must be $\sim \mu v_\infty^2/(\beta_1 GM_1/R_1) \propto v_\infty^2/\beta_1$. On the other hand, even if $v_\infty \ll v_{\rm esc}$, the relative velocity at impact is $\sim v_{\rm esc}$. Recoil shocks are created and lead to the ejection of some shock-heated gas. The amount of mass loss in this regime is nearly independent of v_∞, but depends on the initial stellar structure. Combining both limiting regimes, we expect the *fractional mass loss* $f_{\rm ml} \equiv M_{\rm lost}/(M_1 + M_2)$ in a head-on collision to behave approximately as

$$f_{\rm ml}(r_p = 0) \simeq C_{\rm ml} + D_{\rm ml} \times \frac{v_\infty^2}{\beta_1} , \tag{2.9}$$

where $C_{\rm ml}$ and $D_{\rm ml}$ are constants which depend only on the initial structure of the stars.

For off-axis collisions, the results are much more difficult to predict. No simple analytic expression can be obtained without the help of numerical results. In § 4, we shall discuss our numerical results and derive fitting formulae for mass loss in general stellar collisions.

2.3. *Critical Impact Parameter for Capture*

Stellar collisions can lead to a variety of qualitatively different outcomes, depending on the relative velocity, the periastron separation, and the masses of the stars involved. The two stars can form a bound system after a first dissipative encounter. This bound system should eventually merge into a single

object, although in some cases a detached binary could be formed. Alternatively, the two stars can also remain on a hyperbolic orbit after the encounter, even though some orbital energy has been dissipated and some mass has been lost.

There are two basic mechanisms for forming bound systems or mergers in stellar encounters. One mechanism is *tidal dissipation*, where part of the orbital energy is transferred to small-amplitude stellar pulsations (Fabian et al. 1975). The capture process in this tidal regime has been studied by many authors (Press & Teukolsky 1977; Lee & Ostriker 1986; McMillan, McDermott, & Taam 1987; Ray, Kembhavi, & Antia 1987; Kochanek 1992). The other mechanism is *shock dissipation* in a direct physical collision.

For a given relative velocity v_∞, there is a maximum periastron separation for the formation of a bound system. This *capture radius* $r_{\rm cap}$ decreases as v_∞ increases. For $v_\infty \ll v_{\rm esc}$, $r_{\rm cap}$ may be large enough that there is no physical collision between the stars, and tidal dissipation alone determines whether the stars become bound after their first encounter. In this *tidal regime*, the capture radius $r_{\rm cap}$ scales approximately as

$$r_{\rm cap} \propto v_\infty^{-0.18} , \tag{2.10}$$

for $n = 3$ polytropes with adiabatic index $\Gamma_1 = 5/3$ (Press & Teukolsky 1977; Lee & Ostriker 1986). For low-mass standard models, $\Gamma_1 \simeq 5/3$ and we expect the results of linear perturbation theory to be applicable. Moreover, since the mass distribution in the standard model is very centrally concentrated, we might expect equation (2.10) to hold approximately even for near-grazing-incidence encounters, where only the outer regions of the two stars collide.

In nearly head-on collisions, when $r_p < R_1 + R_2$, the dominant mechanism for dissipating orbital energy is shock heating, which is more efficient in dissipating orbital energy than tidal interaction. Thus we expect the dependence of $r_{\rm cap}$ on v_∞ to steepen in this regime ("collision regime"). This expectation is confirmed by our numerical results (see § 4).

3. NUMERICAL METHOD AND INITIAL SET-UP

Our numerical calculations are based on the smooth-particle hydrodynamics (SPH) method (Lucy 1977; Gingold & Monaghan 1977; see Hernquist & Katz 1989 and Monaghan 1992 for recent reviews). This method is well suited to the study of close stellar encounters in three dimensions. Indeed, the SPH method is completely Lagrangian, wastes no computational resources on empty regions and adapts easily to large distortions of the fluid. Our code has been adapted from that of Rasio & Shapiro (1991, 1992) to allow for the treatment of more general equations of state. Since our goal in this study is to obtain extensive coverage of a large, multidimensional parameter space, we are restricted to a relatively small number of SPH particles and low spatial resolution. All our calculations were done with a total of about 800 SPH particles, with the number of particles for each star proportional to its mass. This relatively small number of particles is not sufficient to study the finer details of the hydrodynamics, but it is adequate for the determination of all global quantities of interest such as energy dissipation and mass loss, to within an accuracy of about 10% (see Steinmetz & Müller 1993). To obtain significantly better spatial resolution, a much larger number of SPH particles, or the use of a three-dimensional finite-difference code would be needed. However, the computation time would then make it prohibitively expensive to obtain good coverage of the parameter space.

We use time-dependent, individual particle smoothing lengths h_i to ensure that the spatial resolution remains acceptable throughout a calculation. This is especially important when using a limited number of particles. The value of h_i is adjusted at every time step so that the number of neighbors that every particle interacts with remains approximately equal to 64. The gravity is calculated by a convolution algorithm, based on fast Fourier transforms (FFT) on a 128^3 grid, which is readjusted at every time step to the mass distribution in the system. A typical run (integrating past the first periastron passage only) takes about 3 CPU hours on an IBM 3090–600J supercomputer. In some cases, we have continued the integration up to the second periastron passage, which requires considerably longer CPU time. Energy and momentum conservation is monitored throughout the integration as a measure of numerical accuracy. In all of our calculations, this conservation was maintained to within a few percent.

In presenting our results, we adopt units such that $G = M_1 = R_1 = 1$, where M_1 and R_1 are the mass and radius of the more massive of the two stars. The corresponding units of velocity and time are

$$\begin{aligned} v_0 &\equiv \left(\frac{GM_1}{R_1}\right)^{1/2} = 436.7\left(\frac{M_1}{M_\odot}\right)^{1/2}\left(\frac{R_1}{R_\odot}\right)^{-1/2} \text{km s}^{-1} , \\ t_0 &\equiv \left(\frac{R_1^3}{GM_1}\right)^{1/2} = 1.594 \times 10^3\left(\frac{M_1}{M_\odot}\right)^{-1/2}\left(\frac{R_1}{R_\odot}\right)^{3/2} \text{s} . \end{aligned} \tag{3.1}$$

The escape velocity from the more massive star M_1 is $v_{\rm esc,1} = 2^{1/2}v_0$. The unit of temperature is

$$T_0 = \frac{GM_1\mu_m m_p}{R_1 k_B} = 1.61 \times 10^7\left(\frac{M_1}{M_\odot}\right)\left(\frac{\mu_m}{0.7}\right)\left(\frac{R_1}{R_\odot}\right)^{-1} \text{K} . \tag{3.2}$$

3.1. *SPH Equations*

The SPH equations we used here are the same as those given in Rasio & Shapiro (1991). However, the equation of state includes both ideal gas pressure and radiation pressure. In the units defined above, this equation of state can be written in dimensionless form as $P = P_{\rm gas} + P_{\rm rad}$, where

$$\begin{aligned} P_{\rm gas} &= \tfrac{2}{3}\rho u_{\rm gas} = \rho T , \\ P_{\rm rad} &= \tfrac{1}{3}\rho u_{\rm rad} = \tfrac{1}{3}\alpha_1^2 T^4 . \end{aligned} \tag{3.3}$$

Here $u_{\rm gas}$ are $u_{\rm rad}$ are the specific thermal energy and radiation energy.

In this work, we integrate the evolution equation for the specific energy $u = u_{\rm gas} + u_{\rm rad}$, rather than using the entropy equation. Note that for a polytropic equation of state, the entropy equation of SPH is to be preferred (Rasio & Shapiro 1992), since the quantity $A_i \equiv P_i/\rho_i^\Gamma$ provides a measure of the specific entropy, which is conserved for adiabatic processes (such as free expansion). Using the entropy equation of SPH then automatically guarantees the conservation of specific entropy in the absence of shocks. However, for a more general equation of state, the expression for the specific entropy can be complicated, and we find it more convenient to integrate the energy equation,

$$\frac{du_i}{dt} = \sum_j m_j\left(\frac{P_i}{\rho_i^2} + \frac{1}{2}\Pi_{ij}\right)(\boldsymbol{v}_i - \boldsymbol{v}_j)\cdot\nabla_i W_{ij} . \tag{3.4}$$

Here Π_{ij} is the artificial viscosity and W_{ij} is the SPH kernel (see Rasio & Shapiro 1991, 1992, for details). Using equation (3.4),

we update the total specific energy u for each SPH particle at every time step. Then the specific thermal energy $u_{\rm gas}$ and radiation energy $u_{\rm rad}$ are obtained by solving the two equations

$$\frac{u_{\rm gas}^4}{u_{\rm rad}} = \left(\frac{3}{2}\right)^4 \frac{\rho}{\alpha_1^2}, \quad u_{\rm gas} = u_{\rm rad} = u\,. \tag{3.5}$$

The first equation in this set was obtained by eliminating T from the two expressions (3.3). In practice, we solve equation (3.5) by iteration, using the values of $u_{\rm gas}$ and $u_{\rm rad}$ at the previous time step as initial guesses. We find that this procedure is very efficient, taking usually just a few iterations to converge.

Although we integrate the energy equation of SPH to evolve the system, we can nevertheless calculate the total entropy of the system as

$$S = \sum_i m_i(s_{{\rm gas},i} + s_{{\rm rad},i}) + S_0\,, \tag{3.6}$$

where S_0 is an arbitrary constant chosen so that $S = 0$ at t = 0. This quantity provides a measure of the amount of shock dissipation during an encounter. The gas entropy and radiation entropy per unit mass for particle i are given by

$$\begin{aligned} s_{{\rm gas},i} &= \frac{3}{2}\frac{k_{\rm B}}{\mu_m m_p}\ln\left(\frac{P_{{\rm gas},i}}{\rho_i^{5/3}}\right), \\ s_{{\rm rad},i} &= \frac{4}{3}\frac{aT_i^3}{\rho_i}, \end{aligned} \tag{3.7a}$$

or, in dimensionless form [with $s_{\rm gas}$ and $s_{\rm rad}$ in units of $k(\mu_m m_p)^{-1}$ and S in units of $k_{\rm B} M_1(\mu_m m_p)^{-1}$],

$$\begin{aligned} s_{{\rm gas},i} &= \frac{3}{2}\ln\left(\frac{2u_{{\rm gas},i}}{3\rho_i^{2/3}}\right), \\ s_{{\rm rad},i} &= \frac{4}{3}\alpha_1^{1/2}\left(\frac{u_{{\rm rad},i}^3}{\rho_i}\right)^{1/4}. \end{aligned} \tag{3.7b}$$

3.2. *Initial Conditions and Set-up*

We specify the stellar masses by giving the mass parameter α_1 (cf. eq. [2.3]) of the more massive component, and the mass ratio $q = M_2/M_1 = \alpha_2/\alpha_1 \leq 1$. The values of β for the two stars are then fixed using equation (2.4). The initial trajectory is specified by the periastron separation r_p and relative velocity at infinity v_∞. For nearly head-on collisions, the two stars are placed at $t = 0$ a distance $d \simeq 2(R_1 + R_2)$ apart. This initial separation is large enough that tidal effects can be ignored in constructing the initial data. For more distant encounters (with $r_p \gtrsim R_1 + R_2$), the two stars are placed further apart initially.

The stars are constructed by placing SPH particles on a cubic lattice and adjusting the particle masses according to the density of a $n = 3$ polytrope (i.e., $m_i \propto \rho_i$). The initial values of the specific energies u, $u_{\rm gas}$ and $u_{\rm rad}$ are obtained from equations (2.2) and (3.3). This procedure has the advantage of maintaining good spatial resolution throughout the star, including near the stellar surface (Rasio & Shapiro 1991). It leads to a more accurate determination of mass losses, since most of escaping gas originates from the outer regions of the stars. Using equal-mass particles and representing the density profile by varying the number density of particles would result in much lower spatial resolution in these outer regions and can lead to large errors in the determination of mass losses.

3.3. *Mass Loss Criteria*

The method we use for determining the amount of gas lost in stellar collisions is similar to that explained in Rasio & Shapiro (1991). First we need to group the particles into different components. This is done as follows. For each particle i and each component n, we calculate the specific enthalpy of the particle with respect to the component as

$$h_i^{(n)} = \frac{1}{2}(\boldsymbol{v}_i - \boldsymbol{v}_{\rm CM}^{(n)})^2 + u_i + \frac{P_i}{\rho_i} + \phi_i\,. \tag{3.8}$$

Here $\boldsymbol{v}_{\rm CM}^{(n)}$ is the center-of-mass velocity of the nth component and ϕ_i is the gravitational potential at $\boldsymbol{r}_i$. Particle i is assigned to the component for which $h_i^{(n)}$ is minimum. If $h_i^{(n)}$ is positive for all components, the particle is part of the escaping gas. Clearly this method must proceed by iterations. In the limit where the various components are well spatially separated and in steady state, the criterion is exact.

In a few cases of very-hyperbolic, nearly head-on collisions that we have calculated, some components are still rapidly expanding at the end of the calculation, and it is difficult to determine whether they are gravitationally bound (see § 4). In those cases we had to supplement the above criterion by calculating approximately the total energy of each component in its center of mass frame as

$$E_{\rm tot}^{(n)} = \sum_i \left[\tfrac{1}{2}m_i(\boldsymbol{v}_i - \boldsymbol{v}_{\rm CM}^{(n)})^2 + m_i u_i + \tfrac{1}{2}m_i\phi_i\right]. \tag{3.9}$$

When $E_{\rm tot}^{(n)} < 0$, we assume that the component will eventually recontract and form a bound object, with no mass lost in the process. Otherwise, we expect it to remain a freely expanding gas cloud, and the mass of this component is then included as part of the mass lost from the system.

To determine how sensitive our results for mass losses are to the number of SPH particles, we have repeated a typical calculation with an increasing number of particles and improving spatial resolution. Specifically, the amount of mass loss in a head-on collision between two stars with $\alpha = 1$ and $v_\infty = 1.187$ was recalculated several times with different numbers of particles. The results are the following: for $N = 2000$ particles, with 32 neighbors per particle, the fractional mass loss $f_{\rm ml} \simeq 11.5\%$; for $N = 4000$, with 32 neighbors, $f_{\rm ml} \simeq 10.0\%$; for $N = 8000$, with 64 neighbors, $f_{\rm ml} \simeq 9.30\%$; for $N = 16{,}000$, with 64 neighbors, $f_{\rm ml} \simeq 8.92\%$; and for $N = 32{,}000$, with 64 neighbors, $f_{\rm ml} \simeq 8.85\%$. We conclude that a calculation using $N = 8000$ particles allows us to determine the fractional mass loss to an accuracy of about 1% of the total mass.

3.4. *Determining the Capture Radius*

The orbital energy after the first periastron passage can be calculated as

$$E'_{\rm orb} = \frac{1}{2}\mu' v_r^2 - \frac{M'_1 M'_2}{r}\,, \tag{3.10}$$

where M'_1 and M'_2 are the masses of the two components after the encounter ($M'_1 < M_1$ and $M'_2 < M_2$ in general), $\mu' = M'_1 M'_2/(M'_1 + M'_2)$, and $\boldsymbol{v}_r$ is the relative velocity of the two components. If $E'_{\rm orb} < 0$, a bound system has formed. The capture radius $r_{\rm cap}$ is determined by the condition $E'_{\rm orb} = 0$ after the first periastron passage, or, equivalently, by $\Delta E = \mu v_\infty^2/2$, where ΔE is the amount of orbital energy dissipated.

Using this procedure, we can determine $r_{\rm cap}$ for encounters with $v_\infty \lesssim v_{\rm esc}$ to within an accuracy of about 10%, given our numerical resources. For very small relative velocity, $r_{\rm cap} \gg R_1 + R_2$ and the amount of energy dissipated is very small and difficult to determine accurately. The smallest relative velocity

for which we have calculated r_{cap} is $v_\infty = 0.173$. To determine r_{cap} accurately for smaller v_∞ would require calculations with much larger numbers of particles. For very high-velocity collisions ($v_\infty > v_{esc}$), the capture radius is also difficult to determine numerically, since these collisions are highly disruptive, and it takes a very long integration time to be able to distinguish between a bound or unbound final state (see § 4.1).

4. NUMERICAL RESULTS

4.1. *Qualitative Outcome of a Collision*

The qualitative outcomes of all our simulations are summarized in Figures 1*a*–1*e*. In these plots, each point corresponds to an encounter with given r_p and v_∞, with different symbols used to distinguish the various types of outcomes. The solid lines show the boundary of the region in parameter space where a bound system is formed. These lines were determined using the criteria discussed in § 3.4. Each plot corresponds to a different combination of stellar masses (specified in terms of α_1 and q). We have performed calculations with $q = 1, 0.5, 0.2, 0.1$, and for $\alpha_1 = 1$, 10 ($M_1/M_\odot \simeq 5$, 50 for $\mu_m \simeq 0.6$–0.7; see eq. [2.3]). These values of masses reflect a reasonable range of parameter space, since only at very high mass ($M \gtrsim 50\ M_\odot$) can radiation pressure start to play a role in the hydrostatic equilibrium of the stars.

4.1.1. *Collisions Between Stars of Equal Masses*

Figure 1*a* summarizes our results for all collisions between two identical MS star with $\alpha = 1$, i.e., with $M_1 = M_2 \simeq 5\ M_\odot$ (for $\mu_m \simeq 0.67$). These represent solar-type stars with $\Gamma_1 \simeq 5/3$

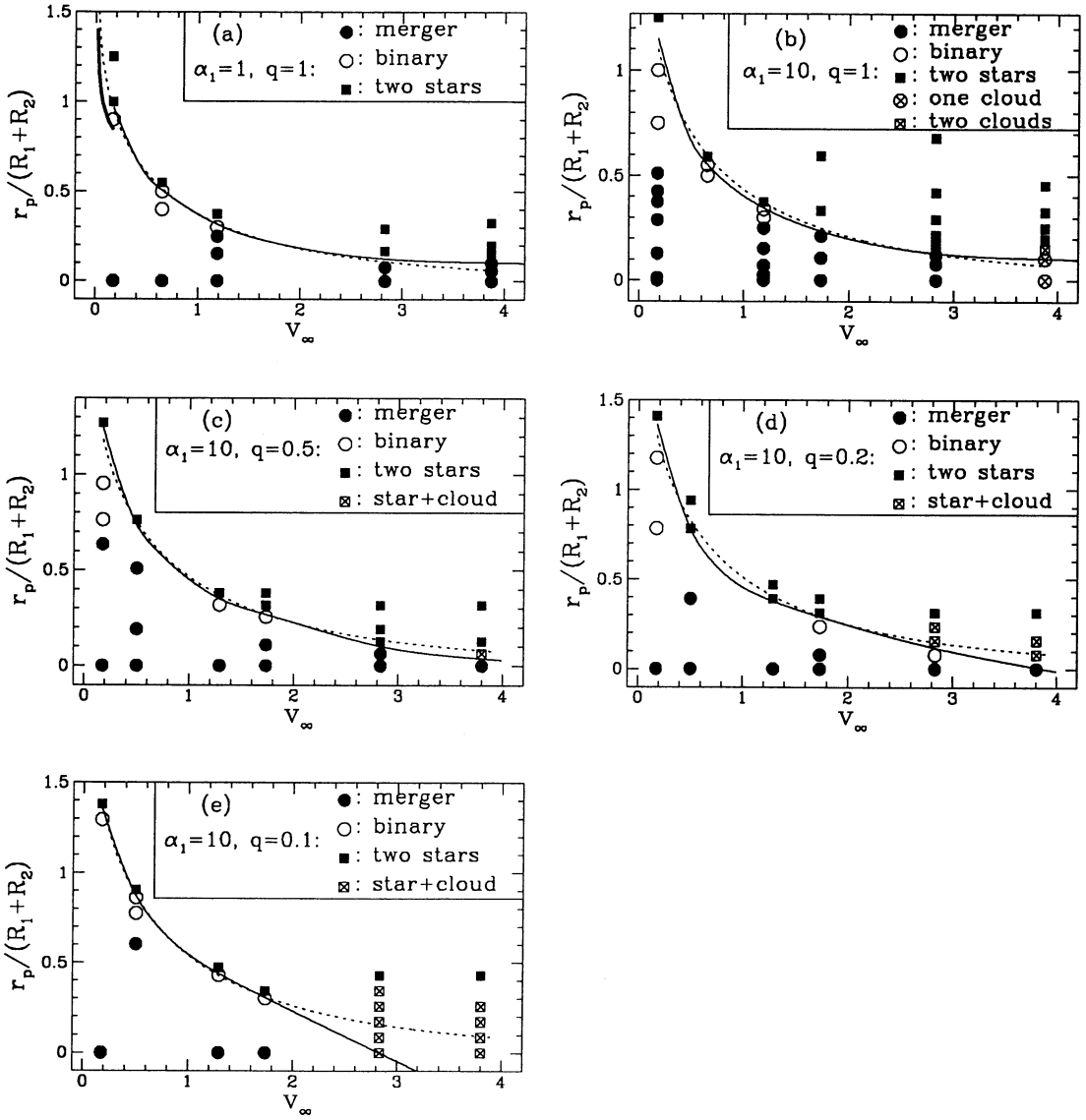

FIG. 1.—Summary of our results for the qualitative outcome of encounters with relative velocity v_∞ [in units of $(GM_1/R_1)^{1/2}$] and periastron distance r_p. Each dot corresponds to a different calculation. Various possible outcomes are specified by different symbols (defined in the figure; see text for details). The different plots correspond to different combinations of the mass parameter α_1 (defined in eq. [2.3]) and the mass ratio $q = M_2/M_1 \leq 1$. The solid lines show the boundary of the region where collisions lead to the formation of a boundary system (merger or binary). The dashed lines are from our numerical fitting formula (eq. [4.6]) for the critical capture radius r_{cap}. (*a*) Collisions of equal-mass stars with $\alpha_1 = \alpha_2 = 1$; (*b*) $\alpha_1 = \alpha_2 = 10$; (c) Collisions of unequal-mass stars: the more massive star has $\alpha_1 = 10$, the mass ratio is $q = 0.5$; (*d*) $\alpha_1 = 10, q = 0.2$; (*e*) $\alpha_1 = 10, q = 0.1$.

and negligible radiation pressure ($\beta = 0.9849$). Figure 1*b* corresponds to $\alpha = 10$ for both stars, i.e., $M_1 = M_2 \simeq 50\ M_\odot$. These are massive MS stars in which radiation pressure is important ($\beta = 0.6721$, $\Gamma_1 = 1.468$). They are much easier to disrupt in a close encounter (cf. eq. [2.8]).

We have carried out calculations for v_∞ ranging from 0.173 to 3.873 (in the units given by eq. [3.1]), corresponding to relative velocity from ~ 75 km s^{-1} to ~ 1700 km s^{-1} The values of $r_p/(R_1 + R_2)$ range from 0 to 1.25. For small enough r_p, the stars merge during their first encounter. Collisions leading to such immediate merging of the two stars are represented by solid round dots in Figure 1 and are labeled "merger." In Figure 2, we show a typical example of such a collision for two stars with $\alpha = 1$. Density contours in the orbital plane are shown at different times. The initial trajectory has $v_\infty = 2.828$ and $r_p = 0.155$. Shock heating of the gas in this nearly head-on collision leads to rapid adiabatic expansion of the merged object for $t > 2$. Some of the material is accelerated to beyond the escape velocity and is lost from the system. Because of angular momentum conservation, the merged object rotates rapidly and sheds some mass from its equator as it recontracts. About 30% of the total mass is lost eventually, and more than half of the initial orbital angular momentum is carried away by the escaping material. As a result, in the end of the calculation, the merged object has a ratio of rotational kinetic energy to gravitational binding energy $T/|W| \lesssim 0.1$, well below the maximum value of $\simeq 0.14$ for stability (see, e.g., Tassoul 1978).

For larger r_p, a smaller fraction of the orbital energy is dissipated and the stars remain on a hyperbolic orbit, although their internal structure may be perturbed quite significantly and some mass may be lost. We have labeled this type of outcome as "two stars" and represented it by solid squares in Figure 1. In Figure 3, we show a typical example of such an encounter. All parameters are the same as in Figure 2 except that $r_p = 0.336R_1$ is slightly larger. The outer regions of the two stars collide and are eventually disrupted with a total mass loss of about 15%. The stellar cores expand somewhat due to shock heating, but they start recontracting adiabatically immediately after the encounter and ultimately retain their identity.

For a narrow range of intermediate values of r_p, a bound system in a highly elliptical orbit is formed after the first encounter. Subsequent periastron passages are likely to

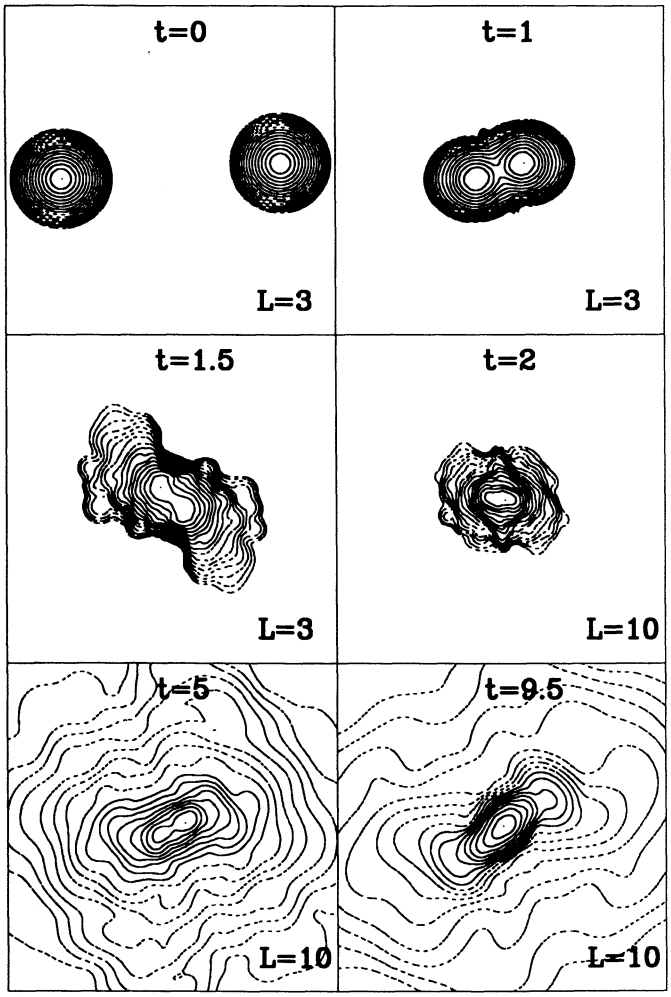

FIG. 2.—Typical encounter leading to one-stage merging. Both stars have $\alpha = 1$, and the initial orbit has $v_\infty = 2.828$ and $r_p = 0.155R_1$. Time t is in units of $(R_1^3/GM_1)^{1/2}$. In each frame, L indicates the length scale, with $-L \le x/R_1$, $y/R_1 \le L$. Density contours in the orbital plane are shown. The 16 contours, spaced logarithmically, cover four decades down from the maximum (the solid-line contours cover the first two decades), i.e., the density of the nth contour is given by $\rho_n/\rho_{\max} = 10^{-n/4}$.

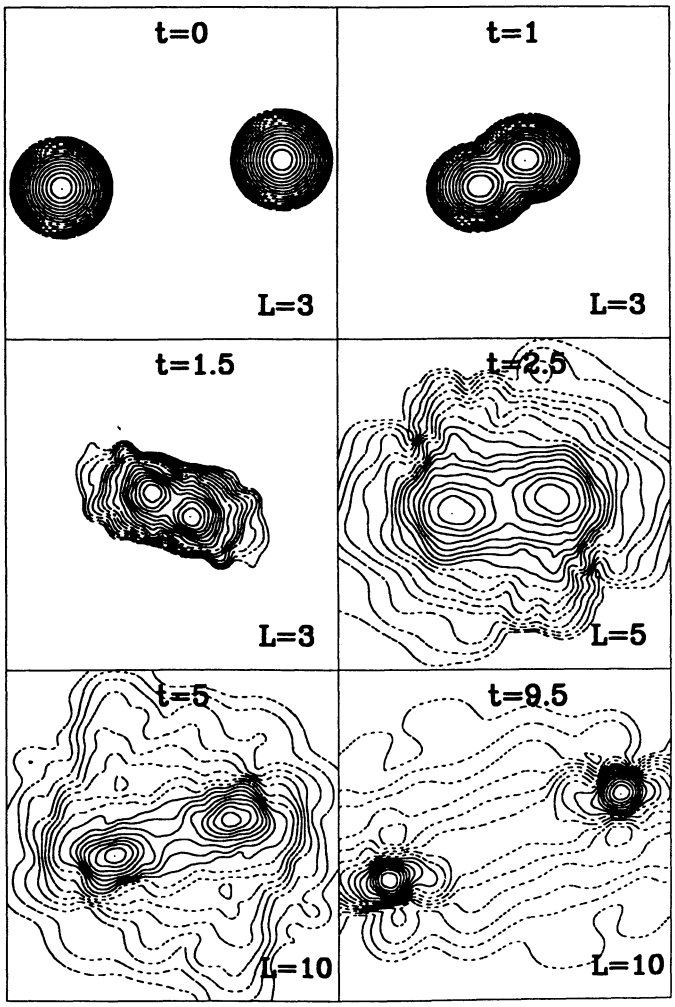

FIG. 3.—Typical encounter between two identical stars with $\alpha = 1$ leading to "two stars" in the end. Here $v_\infty = 2.828$ and $r_p = 0.336R_1$. Conventions are as in Fig. 2.

become more nearly head-on impacts since r_p decreases as a result of dissipation. However, in general, it is computationally very costly to follow the dynamical evolution through a complete orbit and we must terminate the integration soon after the first periastron passage. We label such cases as "binary" in Figure 1 and indicate them as open circles. We emphasize, however, that these may only be short-lived binaries and that we expect eventual merging in most cases (see § 4.4). In a few cases where the first orbital period is sufficiently short we have extended our integration past the second periastron passage to confirm that this merging takes place. An example of such a two-stage merging process is illustrated in Figure 4. The two stars have $\alpha = 1$ and the initial orbit has $v_\infty = 1.187$, $r_p = 0.5R_1$.

To better understand some of the results, we have plotted in Figure 5 the evolution of various global quantities during the encounter depicted in Figure 4. This evolution proceeds most rapidly near periastron. Figure 5*a* shows the evolution of the various energies of the system. Conservation of total energy is maintained to within a few percent. Figure 5*b* shows the total entropy in the system, calculated using expressions (3.6) and (3.7). This quantity provides a measure of shock dissipation in the gas. Figure 5*c* shows the maximum density in the system (*solid line*) and the maximum temperature (*dashed line*) as compared to their initial values. These provide a measure of compression in the system. Clearly, most of the entropy is generated during the first impact, when the system is compressed to high density and temperature, and in the subsequent nonadiabatic recontraction of the two stars. Note that at the end of the dynamical evolution, the merged object has a much smaller density than that of the initial MS stars, but the temperature has changed very little. We find this to be a generic result in all collisions. Although the merged object is not in thermal equilibrium (the Kelvin-Helmhotz time is much longer than the dynamical time), nuclear burning may still be possible immediately after the dynamical phase. During the impact, the temperature can rise to somewhat higher values due to shock heating and compression. This may lead to more rapid nuclear burning. However, the duration of the high-temperature phase is very short and the nuclear energy generation has negligible effect on the hydrodynamics (see also Mathis 1967; Różyczka et al. 1989). In Figure 5*d* we plot the mass fraction of the escaping material as a function of time. We see clearly that most of the escaping material is liberated during the impacts,

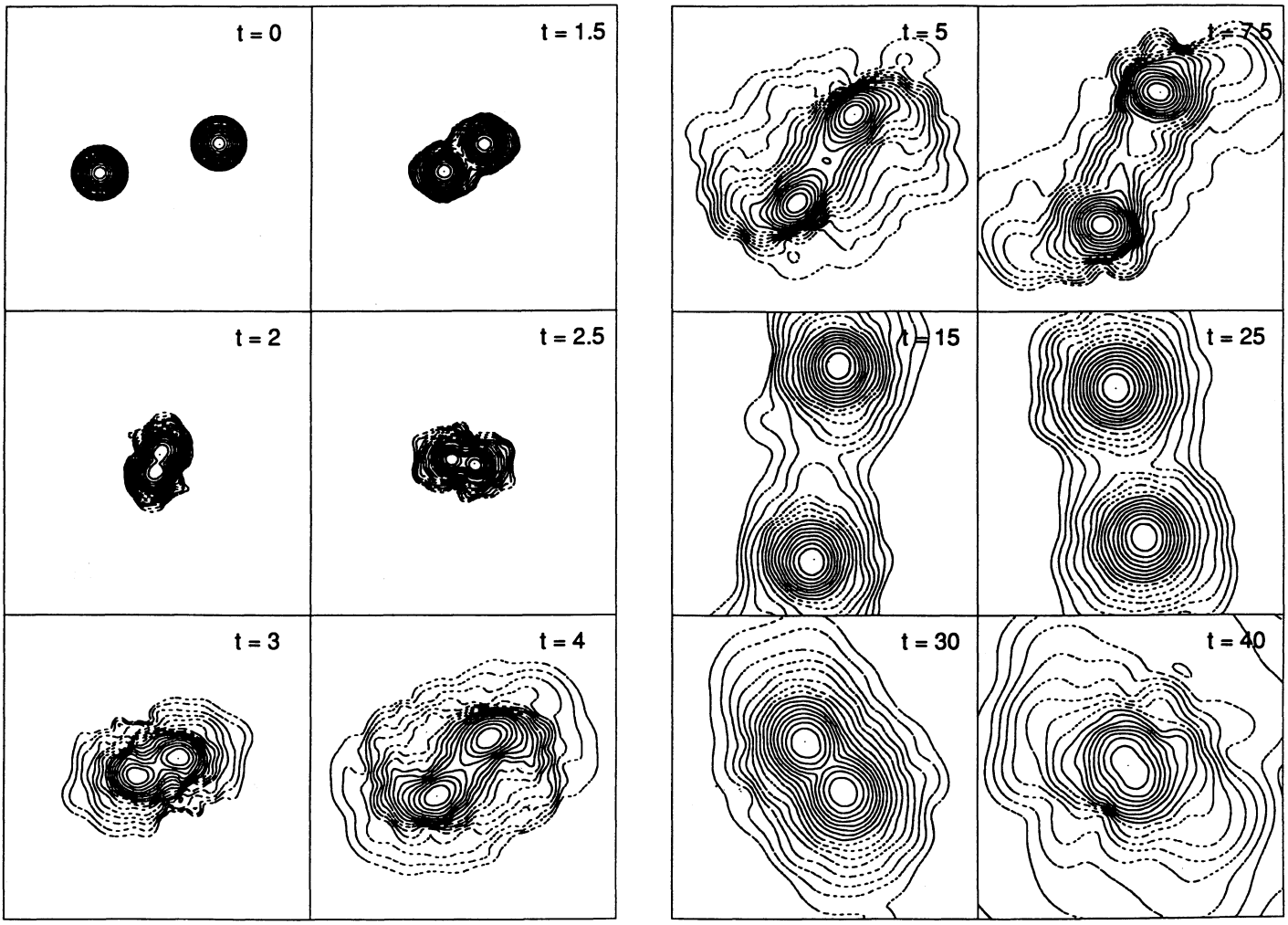

FIG. 4.—Typical encounter leading to a two-stage merging. Both stars have $\alpha = 1$, and the initial orbit has $v_\infty = 1.187$ and $r_p = 0.5R_1$. After the first periastron passage, the two stars become bound in an elliptical orbit. On the second periastron passage, they merge into a single object. Conventions are as in Fig. 2. Here $L = 5$ remains unchanged throughout.

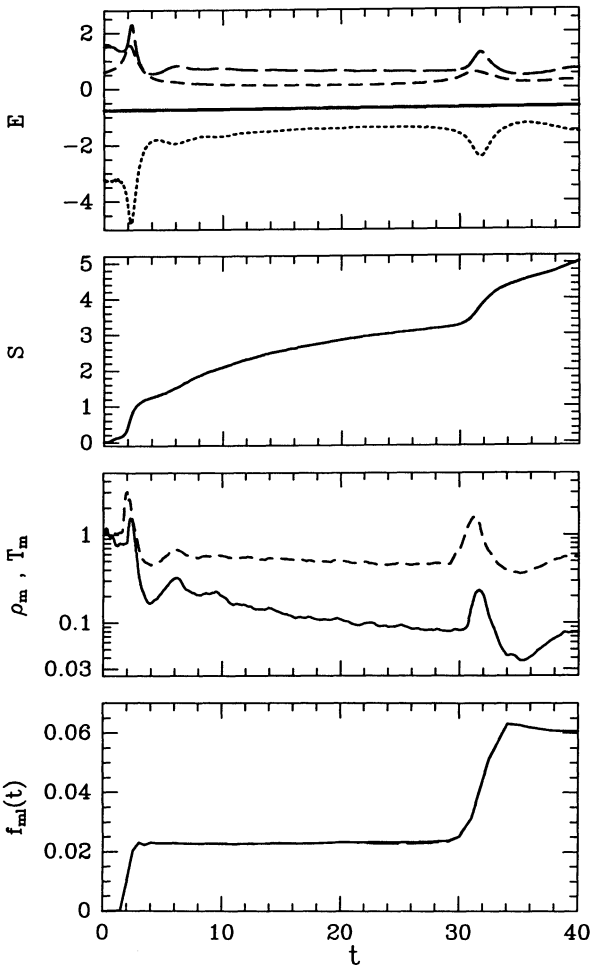

FIG. 5.—Evolution of various global quantities during the collision depicted in Fig. 4. (*a*) Various energies (in units of GM_1^2/R_1): the long-dashed line is the internal energy, the short-dashed line is the kinetic energy, the dotted line is the gravitational potential energy and the solid line is the total (conserved) energy. (*b*) Total entropy [in units of $k_B M_1(\mu_m m_p)^{-1}$] of the gas, calculated from eqs. (3.6) and (3.7). (*c*) The solid line shows the maximum mass density in the system, in units of the initial maximum density; the dashed line shows the maximum temperature in units of the initial maximum temperature. (*d*) The fraction of the total mass that appears to be escaping, determined as explained in § 3.3.

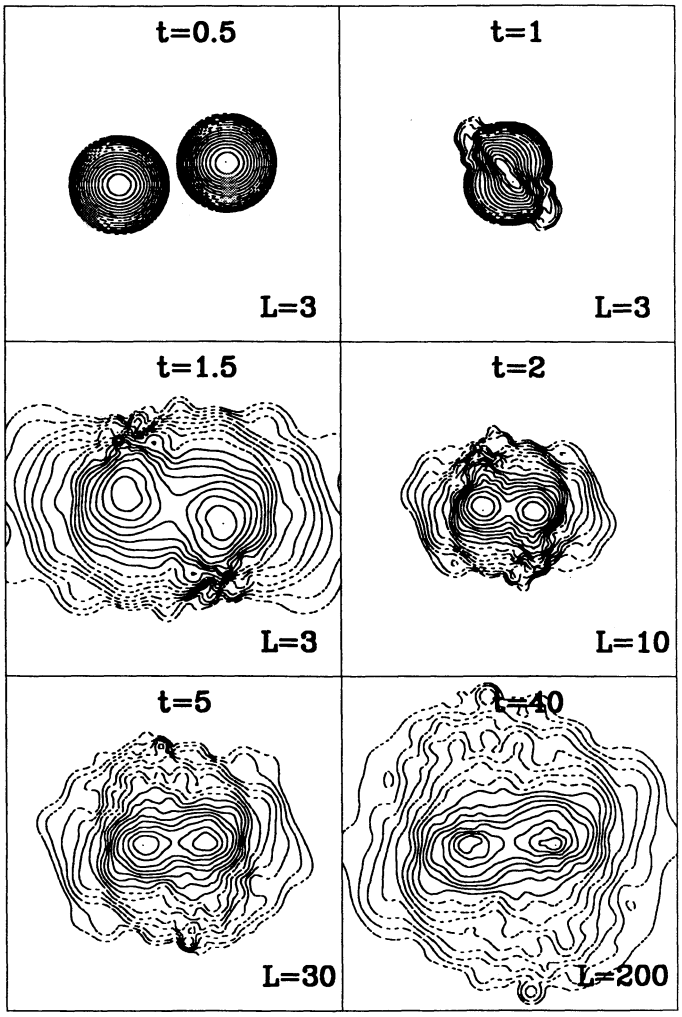

FIG. 6.—Typical high-velocity collision between two identical stars with $\alpha = 10$, leading to complete disruption ("two clouds"). Here $v_\infty = 3.87$ and $r_p = 0.3R_1$. Conventions are as in Fig. 2. At the end the calculation ($t = 40$), the system has expanded by a factor of ~ 100, and the two gas clouds are still expanding.

when strong recoil shocks result in rapid acceleration of the gas. For this particular collision, about 6% of total mass is lost.

At very high velocity ($v_\infty > v_{esc}$), a nearly head-on collision can lead to the rapid and complete disruption of both stars and the formation of either a single or two separate expanding gas clouds. This happens more readily for very massive stars, which are more easily disrupted (see eq. [2.8]). We have observed such outcomes for several collisions between two stars with $\alpha = 10$. They are labeled as "one cloud" or "two clouds" in Figure 1*b*. We note that because of the highly disruptive nature of these collisions, the distinction between those two types of outcome can be difficult to make. Figure 6 shows an example of such a highly disruptive collision between two stars with $\alpha = 10$. The initial trajectory has $v_\infty = 3.87$ ($v_\infty/v_d = 1.93$), and $r_p = 0.3$. At the end of the calculation ($t = 40$), the system has expanded by more than factor of 100 and still shows no sign of recontraction. In Figure 1*b*, this particular case was labeled "two clouds."

4.1.2. *Collisions Between Stars of Unequal Masses*

Figures 1*c*–1*e* summarize our results for collisions between two stars of different masses. The more massive star has a mass parameter $\alpha_1 = 10$ ($M_1 \simeq 50\ M_\odot$ for $\mu_m \simeq 0.7$, and $\beta_1 = 0.672$). The mass ratios considered are $q = 0.5, 0.2$, and 0.1. The corresponding masses of the smaller star are $M_2/M_\odot \simeq 25$, 10, 5 and the values of β are $\beta_2 = 0.819, 0.948, 0.985$, respectively. The impact velocities used in our calculations range from $v_\infty = 0.173$ to $v_\infty = 3.8$ (in the units given in eq. [3.1]), and $r_p/(R_1 + R_2)$ ranges from 0 to 1.4.

Collisions between stars of unequal masses show important new qualitative features, because the less-massive star is also smaller and denser (recall that the mean density $\bar{\rho} \propto M/R^3 \propto M^{-1.4}$). For relatively small v_∞ and r_p ($v_\infty \lesssim v_{esc}$, $r_p \lesssim R_1 + R_2$) the smaller star can penetrate further into the more massive star before losing its identity and merging with the surrounding gas. In Figure 7, we show a typical example of such a collision between two stars of unequal masses ($\alpha_1 = 10$, $q = 0.2$). The initial trajectory has $v_\infty = 0.5$ and $r_p = 0.5R_1$. We see clearly that the smaller star can travel through the outer

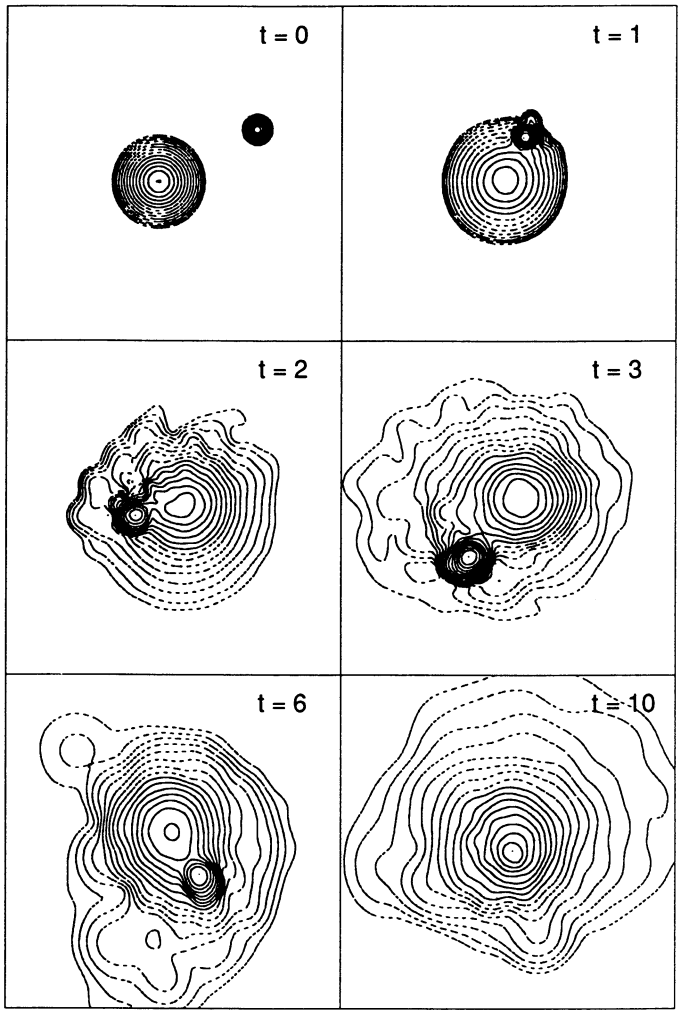

FIG. 7.—Typical collision between two different stars leading to a merger. The more massive star has $\alpha_1 = 10$, and the mass ratio $q = 0.2$. Here $v_\infty = 0.5$ and $r_p = 0.5R_1$. Conventions are as in Fig. 2. Here $L = 3$ remains constant throughout.

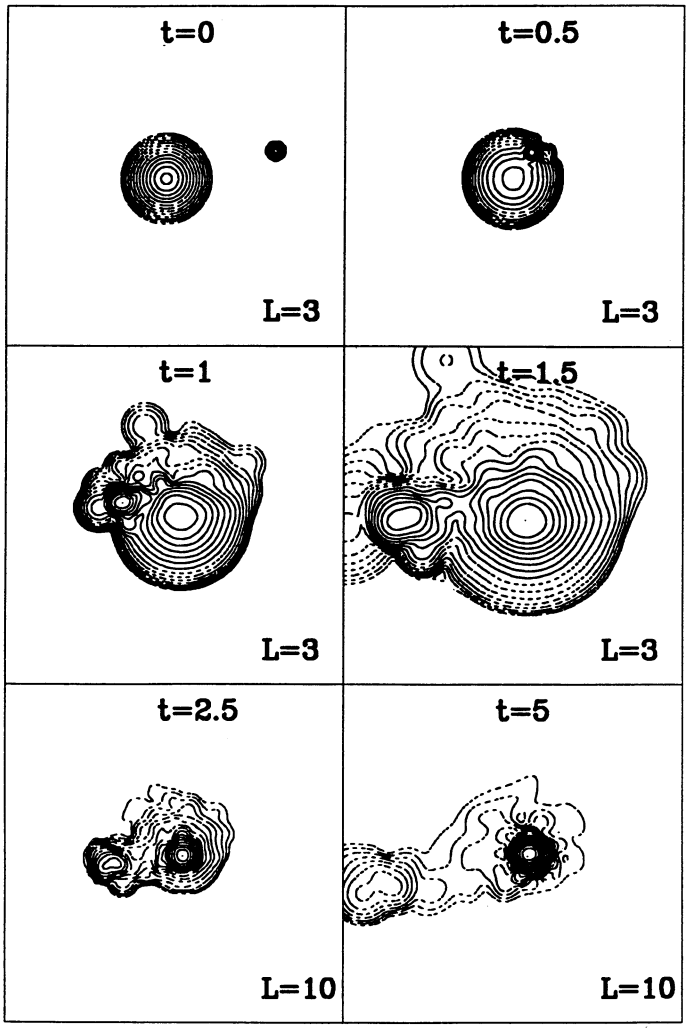

FIG. 8.—Typical collision leading to the complete disruption of one star ("star + cloud"). Here the more massive star has $\alpha_1 = 10$, $q = 0.1$, and the initial orbit has $v_\infty = 2.828$ and $r_p = 0.4R_1$. The smaller star penetrates the more-massive star and emerges as an unbound gas cloud. Conventions are as in Fig. 2.

regions of the more massive star for several dynamical time. Both stars expand and, eventually, the smaller star settles down and merges with the core of the more massive star.

For very high relative velocity ($v_\infty > v_{esc}$), the smaller star can traverse the more massive, lower density star without losing its identity, even for very small impact parameters (Colgate 1967; Sanders 1970; Benz & Hills 1992). However, as it passes through the massive star, the lower mass star still suffers significant shock heating. As a result, it undergoes adiabatic expansion and may eventually become unbound. We have labeled this type of outcome "star + cloud" in Figures 1*c*–1*e*. In Figure 8 we show an example of this type for $\alpha_1 = 10$ and $q = 0.1$. The initial trajectory has $v_\infty = 2.282$ and $r_p = 0.4R_1$. The smaller and denser star penetrates through the outer envelope of the more massive star and disrupts it. Most of the mass loss comes from this initial disruption. After it emerges from the massive star, the smaller star expands adiabatically and becomes an unbound gas cloud. The more massive star also expands as a result of the encounter, but is not completely disrupted. About 14% of the total mass is lost in this collision, with about two thirds of the lost material coming from the envelope of the massive star. The more massive star reaccretes some of the material from the expanding gas cloud so that its final mass is about $0.95M_1$.

Figure 9 shows the evolution of various global quantities during the $q = 0.1$ collision depicted in Figure 8. Before the encounter, the smaller star was about 25 times denser than the massive star. After the encounter, since the smaller star is disrupted, the maximum density in the system is now at the center of the more massive component. The final central density of the massive component is about 4 times smaller than it was initially. In contrast, the central temperature is hardly changed, as already observed in the cases of equal-mass collisions (§ 4.1.1).

In all our calculations of head-on collisions between unequal mass stars, we have never observed a case in which the smaller star could pass through the more massive star and not be disrupted as a result—the smaller star always suffers enough shock heating while passing through the massive star to become unbound. This is in contrast to the results of Benz & Hills (1992) for $n = 3/2$ ($\Gamma_1 = \Gamma = 5/3$) polytropes with $q = 0.2$. The different behavior may result from the higher central concentration of the $n = 3$ polytrope ($\rho_c/\bar{\rho} = 54.2$ for an $n = 3$ polytrope, while $\rho_c/\bar{\rho} = 6.0$ for $n = 3/2$). Indeed, even for a

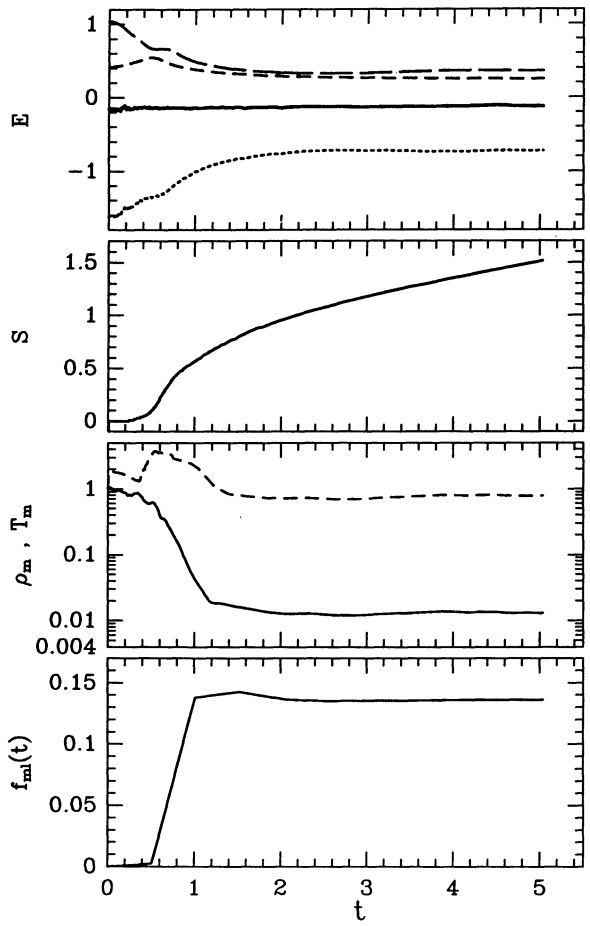

FIG. 9.—Similar to Fig. 5, but for the collision depicted in Fig. 8

mass ratio as small as $q = 0.1$, although the mean density of the smaller star is about 25 times larger than that of the more massive star, the central density of the massive star is still larger than the mean density of the smaller star. Therefore, it seems unlikely that the smaller star could pass through the core of the massive star without being disrupted. Note that this conclusion depends to some extent on the mass-radius relation of the stars. If we choose $R \propto M^{0.55}$ (more appropriate for very massive MS stars), then for $q = 0.1$, the mean density of the smaller star is only 4.5 times that of the more massive star. Thus it is even more unlikely than the smaller star can penetrate through the core of the more massive star without being disrupted. While it may still be possible for an even smaller star to survive a head-on collision with relative velocity $v_\infty \gg v_{esc}$ (Colgate 1967), we do not explore this possibility here. Finally, we note that, in the case of small mass ratio, although the mean densities of the two stars are very different, their specific binding energies are comparable (they mainly differ by a factor of β; see eq. [2.5]). For example, the specific binding energies of a 1 $M_\odot$ star and a 50 $M_\odot$ star differ by less than a factor of 2. Therefore, representing the low-mass star by a point mass (as done by Benz & Hills 1992) may not be a good approximation.

4.2. *The Capture Radius*

As discussed in § 2, for a given relative velocity v_∞, there exists a critical periastron separation r_{cap} for the formation of a bound system. In Figure 1, the solid lines show the variation of r_{cap} (determined as explained in § 3.4) as a function of v_∞. In Figure 10, we plot these r_{cap}–v_∞ curves on a logarithmic scale for two mass combinations: $\alpha_1 = 1, q = 1$ and $\alpha_1 = 10, q = 0.1$. The curves for other mass combinations that we have calculated lie between the two curves shown in Figure 10.

4.2.1. *The Tidal Regime*

It is interesting to compare our results for the capture radius with the predictions of linear perturbation theory of tidal capture. The orbital energy dissipated in a star of mass M_1 and radius R_1, during a tidal encounter with a star of mass M_2 and radius R_2 is approximately given by

$$\Delta E_{tide}(M_1) \simeq f \frac{GM_2^2}{R_1}\left(\frac{R_1}{r_p}\right)^6 , \tag{4.1}$$

where r_p is the periastron distance and f is a dimensionless factor of order unity (Fabian et al. 1975). A similar expression can be obtained for $\Delta E_{tide}(M_2)$. Clearly, tidal dissipation in the more massive star is dominant. The critical radius for capture r_{cap} is determined by the condition that $\Delta E_{tide} \simeq \mu v_\infty^2/2$, which gives

$$\frac{r_{cap}}{R_1 + R_2} \simeq f^{1/6} \frac{q^{1/6}}{(1+q)^{5/6}} v_\infty^{-1/3} . \tag{4.2}$$

More detailed calculations of tidal capture using linear perturbation theory indicate that $f \propto r_p^{-5}$, i.e., $\Delta E_{tide} \propto r_p^{-11}$ (Press & Teukolsky 1977; Lee & Ostriker 1986). This implies $r_{cap} \propto v_\infty^{-0.18}$. For two identical $n = 3$ polytropes with adiabatic index $\Gamma_1 = 5/3$, the result of Lee & Ostriker (1986) can be fitted approximately by the following expression:

$$\frac{r_{cap}(LO)}{R_1 + R_2} = 0.575\left(\frac{v_\infty}{v_{esc}}\right)^{-0.18} = 0.612 v_\infty^{-0.18} . \tag{4.3}$$

A standard model MS star with $\alpha = 1$ has the density profile of an $n = 3$ polytrope and an adiabatic index $\Gamma_1 = 1.644 \simeq 5/3$. Therefore we expect that our values of r_{cap} for low-velocity

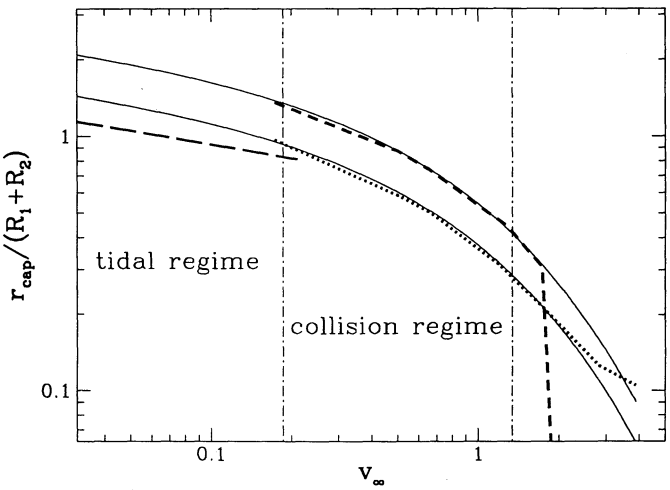

FIG. 10.—The capture radius r_{cap} as a function of relative velocity v_∞, determined using the method of § 3.4. The dotted line is for $\alpha_1 = 1$, $q = 1$, and the dashed line is for $\alpha_1 = 10$, $q = 0.1$. The solid lines show our fitting formula (eq. [4.4]). The long-dashed line on the left shows the tidal capture radius obtained from linear perturbation theory (eq. [4.3]). For small v_∞, to the left of the first vertical line, tidal dissipation dominates in the capture process ("tidal regime"), while for larger v_∞, shock dissipation dominates ("collision regime"). At very high velocity, collisions are very disruptive and the numerical values for r_{cap} are not well determined (see text).

collisions between two stars with $\alpha = 1$ should approach those given by equation (4.3). Indeed, for encounters with $v_\infty = 0.178$ (the smallest value we considered), the critical capture radius $r_{cap} \gtrsim R_1 + R_2$. Although the outer envelopes of the stars collide, shock dissipation is negligible since the density profiles ($n = 3$ polytrope) are so centrally concentrated. In Figure 1*a* and Figure 10, we see that our numerical curves do indeed appear to converge to the Lee-Ostriker result (eq. [4.3]) for small v_∞. For $v_\infty = 0.173$, the two results differ by about 10%, but the power-law scaling of our curves in the low-velocity limits is very close to that of equation (4.3). Limited numerical resolution makes it difficult to determine r_{cap} for a collision with smaller v_∞ (see § 3.4).

When $r_p \lesssim R_1 + R_2$, the differences between our numerical results and those obtained from linear theory increase, indicating the breakdown of the linear approximation. At small r_p, linear theory tends to underestimate the tidal energy dissipation by a factor of a few. This fact was also demonstrated by Rasio & Shapiro (1991) using SPH simulations of polytropes, and by Kochanek (1992) and Kosovichev & Novikov (1992) using the affine model of Carter & Luminet (1985). However, note that r_{cap} is not very sensitive to the exact amount of tidal dissipation. Indeed, since $\Delta E_{tide} \propto r_p^{-11}$, even if ΔE_{tide} is underestimated by a factor of 2, the value of r_{cap} is hardly changed. Thus the linear theory can still give reasonably accurate r_{cap}.

Our results for the capture of stars with $\alpha = 10$ show larger deviations from those of Lee & Ostriker (1986). This is in part because $\Gamma_1 = 5/3$ is assumed in their calculation, while $\Gamma_1 = 1.468$ for a standard model with $\alpha = 10$. The value of Γ_1 affects the structure of the stellar pulsation modes which are excited during a tidal interaction. New calculations of the tidal capture mechanism using the method of Press & Teukolsky (1977) for polytropes with $\Gamma_1 < 5/3$ would be useful.

4.2.2. *The Collision Regime*

For encounters with larger relative velocity v_∞, tidal dissipation is not sufficient to form a bound system and we find that $r_{cap} < R_1 + R_2$. In this collision regime, shock dissipation is the dominant mechanism for capture. In Figure 10, we see that as v_∞ increases and r_{cap} decreases, the dependence of r_{cap} on v_∞ becomes much steeper than in the tidal regime. Our numerical calculations provide a smooth transition from the tidal regime to the collision regime. For very high relative velocity ($v_\infty > 2.4$, or $v_\infty/v_{esc} > 1.7$), it can be difficult to determine precisely the final outcome of a collision, especially for r_p near r_{cap}. This is because of the nearly complete disruption of the stars (see the discussion at the end of § 4.1.1 and Fig. 6). Although our results for r_{cap} are uncertain in this limit, this is rather unimportant since very little mass is left in the bound, merged object.

4.2.3. *Fitting Formulae*

Our numerical results for the capture radius r_{cap} can be fitted approximately by the following relation:

$$\frac{r_{cap}}{R_1 + R_2} \simeq A_{cap}(\alpha_1, q)\left(\frac{0.173}{v_\infty}\right)^\eta , \tag{4.4a}$$

with

$$\eta = 0.18 + \left(\frac{v_\infty}{8}\right)^{1/2} , \tag{4.4b}$$

where v_∞ is in the units of equation (3.1) and A_{cap} is a dimensionless coefficient depending on the masses of the two colliding stars. The values of A_{cap} are listed in Table 1 for different mass combinations. The exponent η in equation (4.4) has been chosen so that the limiting scaling of equation (4.3) is recovered in the $v_\infty \ll 1$ limit ("tidal regime"). At the same time, the steepening of the r_{cap} versus v_∞ relation in the high velocity collision regime due to higher efficiency of shock heating in dissipating the orbital energy can be modeled by the dependence of η on v_∞ introduced in expression (4.4b). In Figure 1, the fitted curves are shown as dotted lines. We find that expression (4.4) can fit all our numerical results to within about 10% for $v_\infty \lesssim 2.4$. At higher relative velocity, the hydrodynamics is more complicated and equation (4.4) no longer applies.

TABLE 1

FITTING PARAMETERS[a]

	α_1				
PARAMETER	1	10	10	10	10
β_1	0.9849	0.6721	0.6721	0.6721	0.6721
$q = M_2/M_1$	1	1	0.5	0.2	0.1
A_{cap}	0.95	1.10	1.18	1.30	1.38
C_{ml}	0.06	0.06	0.05	0.02	0.002
D_{ml}	0.0120	0.0120	0.0127	0.0125	0.010
A_{ml}	0.50	0.50	0.55	0.67	0.90
ΔA_{ml}	0.075	0.075	0.12	0.13	0.14

[a] α_1 is the mass parameter (defined in eq. [2.3]) of the more massive star ($\alpha_1 = 1$ corresponds to a mass $M_1 \simeq 5\ M_\odot$ for $\mu_m = 0.6$–0.7). The value of β is determined from eq. (2.4). The parameter A_{cap} is used in the critical capture radius r_{cap} (eq. [4.4]), C_{ml} and D_{ml} are used in the expression for the fractional mass loss from head-on collisions (eq. [4.7]), A_{ml} and ΔA_{ml} appear in eq. (4.10), which is used in the fitting formula for the fractional mass loss in off-axis collisions (eq. [4.9]).

The dependence of the coefficient A_{cap} on the masses of the two stars (Table 1) can be fitted quite accurately by the expression

$$A_{cap}(\alpha_1, q) = A_{cap}(\alpha_1, q = 1)/q^{0.10} . \tag{4.5}$$

From Table 1, we see that $A_{cap}(\alpha_1, q = 1) \simeq 1$, and that it increases with α_1. While we give no theoretical justification for this simple expression, we point out that this power-law scaling with q is very different from that expected from simple tidal break-up considerations. Indeed, setting r_{cap} equal to the critical binary separation for "Roche lobe overflow" would give $r_{cap}/R_1 \propto (1 + q)^{1/3}$, or $A_{cap} \propto (1 + q)^{1/3}/(1 + q^{0.8})$, a much steeper dependence than indicated by our numerical results. The dependence of A_{cap} on q for $\alpha_1 = 10$ is illustrated in Figure 11.

4.3. *The Mass-Loss Fraction*

4.3.1. *Head-on Collisions*

In § 2.2, we have discussed some qualitative features of mass losses from head-on collisions. Clearly, an expression such as equation (2.9) is a rather crude approximation which ignores some of the complicated hydrodynamic processes leading to mass losses. Nevertheless, we might expect the fractional mass loss in a head-on collision to exhibit a similar dependence on v_∞^2/β_1 (as in eq. [2.9]); we also expect the mass loss fraction to depend on the reduced mass $\mu \propto 2q/(1 + q)$, reflecting the available energy μv_∞^2, and also on the mass ratio q, reflecting the fraction of effective collision region of the stars. Thus we have attempted to fit our numerical results by the following

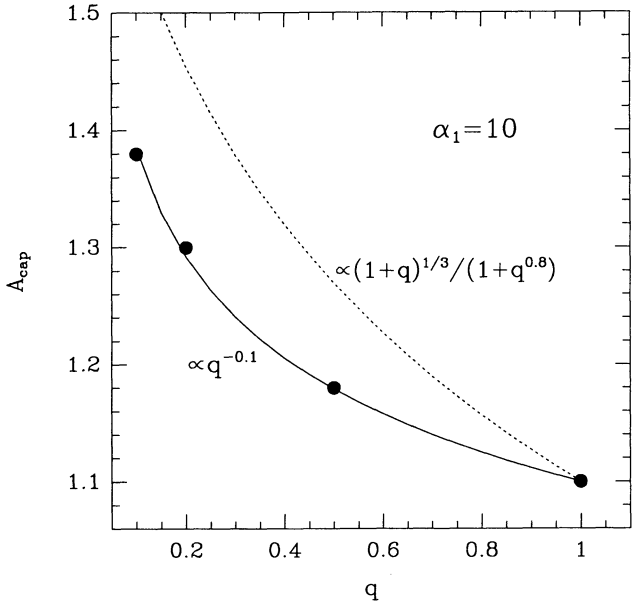

FIG. 11.—Variation of the fitting parameter A_{cap} (cf. eq. [4.4]) with mass ratio. Here $\alpha_1 = 10$ is fixed. The solid line is from eq. (4.5). The dashed line shows the variation expected from a simple Roche-lobe-type model (see text for details).

expression

$$f_{ml}(r_p = 0) = C_{ml}(\alpha_1, q) + D_{ml}(\alpha_1, q)\left(\frac{v_\infty^2}{\beta_1}\right)^{v_1}\left(\frac{2q}{1+q}\right)^{v_2} q^{v_3}, \quad (4.6)$$

where the exponents v_1, v_2, and v_3 are constants, and C_{ml}, D_{ml} depend only on the masses of the two stars.

Our numerical results for mass losses are illustrated in Figure 12 for various mass combinations. Figure 12*a* shows $f_{ml}(r_p = 0)$ as a function of v_∞ for two identical stars with $\alpha = 10$ or $\alpha = 1$, while Figure 12*b* compares the results for different mass ratios when the more massive star has fixed $\alpha_1 = 10$. Fitting these numerical results with the expression (4.6), we obtain

$$f_{ml}(r_p = 0) = C_{ml}(\alpha_1, q) + D_{ml}(\alpha_1, q)\left(\frac{v_\infty^2}{\beta_1}\right)^{1.4}\left(\frac{2q}{1+q}\right)^{0.4} q^{0.2}, \quad (4.7)$$

with the values of the coefficients C_{ml} and D_{ml} given in Table 1 for various combinations of masses. In Figure 12, the lines show the results of our fitting formula equation (4.7) using the parameters in Table 1. This fit is accurate to within about 20% (i.e., $\delta f_{ml}/f_{ml} \lesssim 20\%$) when $f_{ml} \gtrsim 5\%$, while the error on f_{ml} can be a few percent of the total mass when $f_{ml} \lesssim 5\%$ (recall that the typical numerical error bar for mass loss is $\delta f_{ml} \sim 1\%$, see § 3.3).

We note from Table 1 that the coefficient $D_{ml} \simeq 0.012$, almost independent of the masses. At the same level of approximation, we can fit the coefficient C_{ml} approximately as $C_{ml} \simeq 0.06q^{1.2}(2q)^{0.4}/(1+q)^{0.4}$. Combining these expressions, we get

$$f_{ml}(r_p = 0) \simeq \left[0.06q + 0.012\left(\frac{v_\infty^2}{\beta_1}\right)^{1.4}\right]\left(\frac{2q}{1+q}\right)^{0.4} q^{0.2}. \quad (4.8)$$

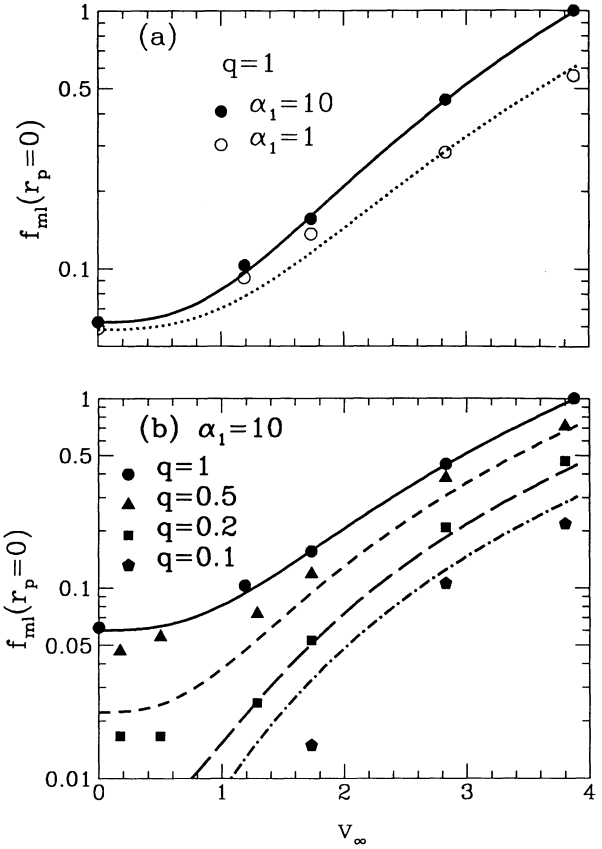

FIG. 12.—Mass-loss fraction in head-on collisions. The dots show our numerical results. The lines are from our fitting formula, expression (4.7), with parameters given in Table 1. (*a*) Equal-mass collisions with $\alpha_1 = 10$ and $\alpha_1 = 10$ and $\alpha_1 = 1$. (*b*) Collisions with different mass ratios, $q = 1$, 0.5, 0.2, 0.1, where the more-massive star has $\alpha_1 = 10$.

We find that equation (4.8) can be used to predict the mass loss fraction in any head-on collision to within an accuracy of about 30%.

4.3.2. *Off-axis Collisions*

The numerical results for mass losses from collisions with $r_p \neq 0$ are much more complicated. In Figure 13*a*–13*e*, we show the fractional mass loss f_{ml} as a function of periastron distance r_p for different relative velocities v_∞ and five different combinations of masses. We see that the behavior of f_{ml} can be quite complex. In particular, f_{ml} does not always decrease monotonically as r_p increases. This arises mainly from two different effects. One is that, as we noted before, for some intermediate values of r_p, a short-lived detached binary forms after the first periastron passage and merging takes place only after a subsequent periastron passage. In these cases, shock heating is enhanced and more mass is lost than in a one-stage merging. The same behavior has been noticed by Benz & Hills (1987) in their simulations of collisions between $n = 3/2$ polytropes. The effect is especially pronounced for low-velocity collisions such as those shown in Figure 13*b* for two equal-mass stars with $\alpha_1 = 10$ and $v_\infty = 0.173$. The second effect is that, for $r_p \neq 0$, the high-density central region of one star tends to collide with the low-density envelope of the other. In such cases, a significant fraction of the infall kinetic energy of the colliding fluid elements still remains after the impact, and the net impulse

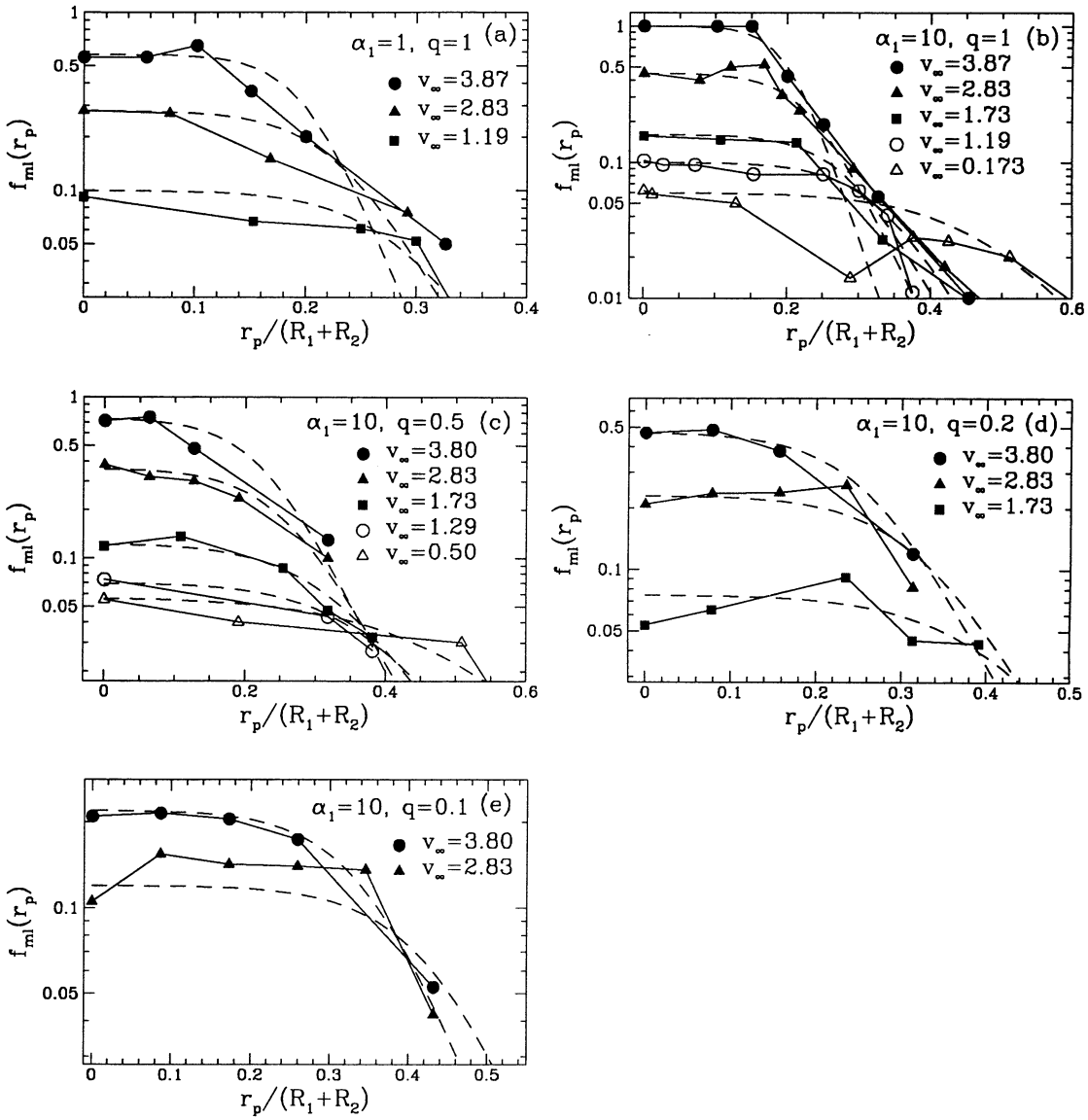

FIG. 13.—Fractional mass loss $f_{ml}(r_p)$ for general off-axis collisions of stars with different combinations of masses. The dots show our numerical results, with different symbols indicating different values of the relative velocity v_∞. The dashed lines are from our fitting formulae, expressions (4.7), (4.9), and (4.10) with parameters given in Table 1.

imparted by the higher density fluid elements can easily eject the lower density fluid elements in the other star. This effect is dominant for high-velocity collisions between unequal masses, such as the $\alpha_1 = 1$, $q = 1$ collisions with $v_\infty = 3.87$ in Figure 13*a*, $\alpha_1 = 10$, $q = 1$ collisions with $v_\infty = 2.83$ in Figure 13*b*, and $\alpha_1 = 10$, $q = 0.2$ collisions with $v_\infty = 2.83$ in Figure 13*f*.

Combining all the numerical results for mass losses in off-axis collisions into a simple analytical fitting formula is clearly a difficult task. However, there is at least one generic feature reflected in Figure 13 that we can model easily: in all cases, there is a characteristic periastron distance r_{ml}, below which f_{ml} remains approximately constant and equal to $f_{ml}(r_p = 0)$. For $r_p \gtrsim r_{ml}$, f_{ml} decreases rapidly in most cases. This motivates a fit to a Fermi-Dirac-type function,

$$f_{ml}(r_p) = \frac{f_{ml}(r_p = 0)}{\exp\left[(r_p - r_{ml})/\Delta r_{ml}\right] + 1}, \qquad (4.9)$$

where Δr_{ml} is a parameter measuring the width of the transition around $r = r_{ml}$. The dependence of the parameters r_{ml} and Δr_{ml} on v_∞ is shown in Figure 14 for different values of q. Their dependence on the mass parameter α is too weak to be determined numerically given our numerical accuracy. Thus we assume that r_{ml} and Δr_{ml} are functions of q and v_∞ only. The dashed lines in Figure 13 show the variation of f_{ml} as predicted by equation (4.9). We used the values of r_{ml} and Δr_{ml} given in Figure 14, and calculated $f_{ml}(r_p = 0)$ from equation (4.7). We see that equation (4.9) provides a reasonable estimate of the mass losses, although it does not reproduce all the details of our numerical results.

The critical mass-loss radius r_{ml} and the parameter Δr_{ml} are somewhat related to the critical capture radius r_{cap} discussed in § 4.2. Indeed, for a near-grazing collision leading to "two stars" (see § 4.1), only the outer layers of the stars suffer physical collision and mass loss is relatively small. Instead, for a

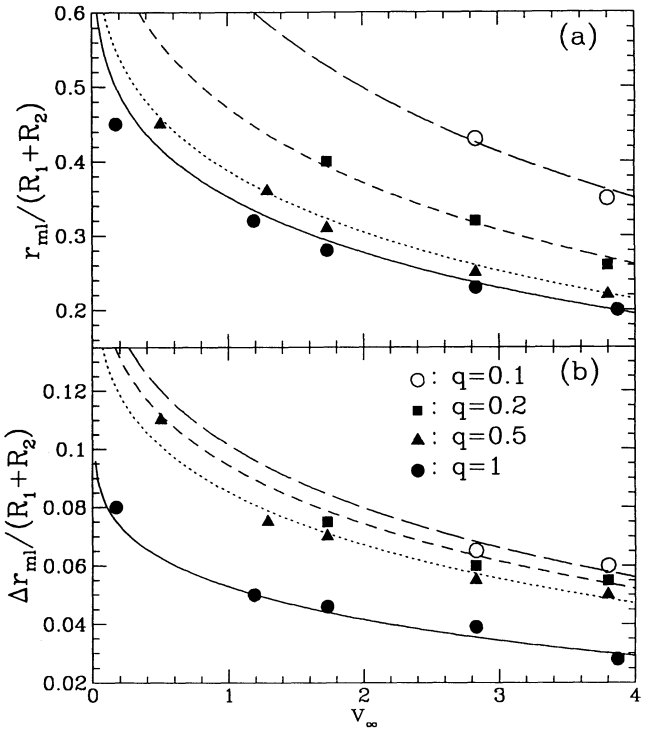

FIG. 14.—Variation of the fitting parameters r_{ml} and Δr_{ml} (cf. eq. [4.9]) with relative velocity. The dots show the best choices of r_{ml} and Δr_{ml} that fit the mass loss with expression (4.9) for different mass ratios. The lines show the fit to the dependence of r_{ml} and Δr_{ml} on v_∞ with expressions (4.10).

nearly head-on collision leading to a merger, the entire volume of the stars undergo shock heating and, as a result, more mass is lost. Thus, in analogy with expression (4.4) for r_{cap}, we have tried to fit the variation of r_{ml} and Δr_{ml} in Figure 14 with the expressions

$$\frac{r_{ml}}{R_1 + R_2} = A_{ml}\left(\frac{0.173}{v_\infty}\right)^{\delta}, \tag{4.10a}$$

and

$$\frac{\Delta r_{ml}}{R_1 + R_2} = \Delta A_{ml}\left(\frac{0.173}{v_\infty}\right)^{\delta}, \tag{4.10b}$$

where

$$\delta = \frac{1}{10}(1 + v_\infty^{1/2}). \tag{4.10c}$$

The coefficients A_{ml} and ΔA_{ml} are functions of the mass ratio only. Their values are given in Table 1 and the corresponding fitted curves for r_{ml} and Δr_{ml} are plotted in Figure 14.

The set of expressions (4.7)–(4.10) together with Table 1 provides a simple recipe for predicting the mass loss fraction in any collision between two MS stars. The overall accuracy of these fitting formulae for f_{ml} is about 30%, except when f_{ml} is small ($\lesssim 5\%$), in which case the absolute error in f_{ml} remains a few percent of the total mass. These results should prove very useful for incorporating approximately the effects of mass losses from stellar collisions in dynamical simulations of dense stellar systems.

4.4. *Merger or Binary?*

For sufficiently large velocity $v_\infty \gtrsim 1$, we have seen that capture necessarily involves physical collision between the two stars. In this case, the stars merge during the first periastron passage ("one-stage merging") and $r_{mrg} = r_{cap}$. However, for small enough relative velocity, tidal capture can occur with no physical collision at all. In this case, a highly eccentric, initially detached binary is formed. The final fate of the binary depends on the dissipation of orbital energy during successive periastron passages. Since the periastron distance keeps decreasing from one periastron passage to the next, and since the stellar radii keep increasing in response to the dissipation, we expect the stars to collide and merge eventually. The critical radius for merging in this regime is therefore $\gtrsim (R_1 + R_2)$. In general, we write the critical periastron distance for merger, r_{mrg}, as

$$r_{mrg} = \min\,[r_{cap}\,,\ C(R_1 + R_2)]\,, \tag{4.11a}$$

or

$$r_{mrg} = \begin{cases} C(R_1 + R_2)\,, & \text{if } v_\infty < v_{mrg}\,; \\ r_{cap}\,, & \text{if } v_\infty \geq v_{mrg}\,. \end{cases} \tag{4.11b}$$

Here C is a constant of order unity, and v_{mrg} is defined by setting $C(R_1 + R_2) = r_{cap}(v_{mrg})$.

In a few cases, we have carried out a calculation through a two-stage merger process. One example was shown in Figure 4 for two identical stars. Another example, for two stars of different masses ($\alpha_1 = 10$, $q = 0.5$) and with small relative velocity ($v_\infty = 0.173$), is shown in Figure 15. The initial periastron separation $r_p = R_1 = 0.64(R_1 + R_2)$. This example clearly demonstrates that $C > 0.64$, based on the merging after the second close passage. We expect the actual value of C to be considerably larger, since final merging may take place only after a large number of close passages if the energy dissipated during each close passage is very small. In the following discussion, we adopt $C = 1$ for definiteness.

An estimate of r_{mrg} when $v_\infty \ll v_{esc}$ has been given by Lee & Ostriker (1986). For equal mass $n = 3$ polytropes, they find $r_{mrg}(\mathrm{LO}) \simeq 0.53R$. This result comes from considering the maximum angular momentum that a stable merged configuration can sustain, and assumes that no mass or angular momentum is lost from the system. However, our numerical results show that some mass and angular momentum is always lost during a merger (cf. § 4.1.1). Of particular importance is that the *specific angular momentum* of the escaping material is always larger than that of the entire system initially, leading to an efficient reduction of the ratio $T/|W|$ for the bound component. The result of Lee and Ostriker is therefore too conservative.

5. APPLICATIONS TO STELLAR CLUSTERS

Using the results of § 4, we now estimate various cross sections and rates related to collisions between MS stars in a dense cluster.

5.1. *Cross Sections*

Consider a star of mass M_1 and radius R_1 approaching another star of mass M_2 and radius R_2, with relative velocity v_∞. The impact parameter b is given by

$$b^2 = (R_1 + R_2)^2\left(x_p^2 + x_p\frac{2}{v_\infty^2}\right), \tag{5.1a}$$

where we have defined

$$x_p \equiv \frac{r_p}{R_1 + R_2}\,. \tag{5.1b}$$

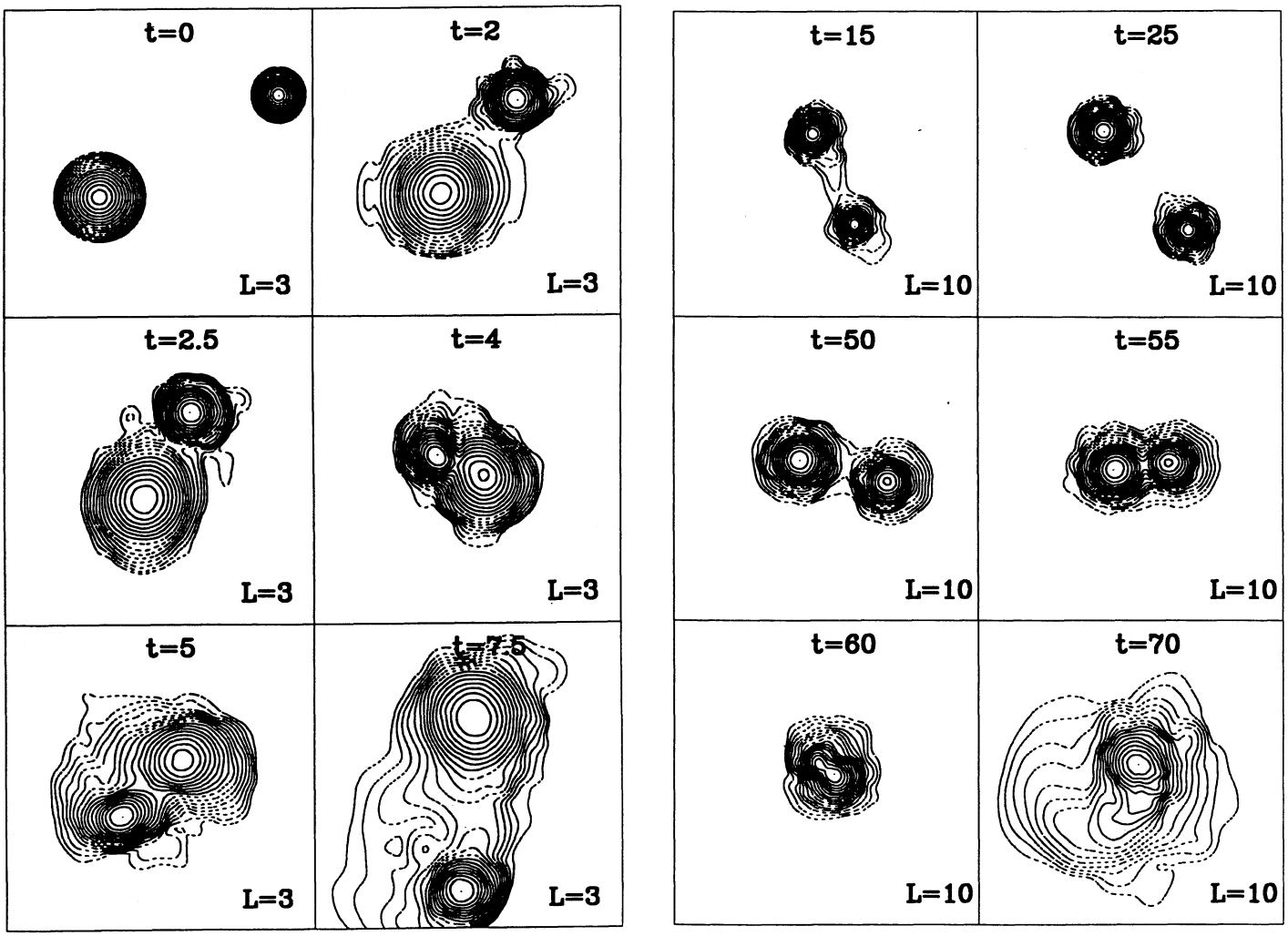

FIG. 15.—Two-stage merging for a collision between two stars of unequal masses with $v_\infty = 0.173$ and $r_p = R_1$. The more massive star has $\alpha_1 = 10$, and the mass ratio $q = 0.5$. This collision has the largest value of $r_p/(R_1 + R_2) = 0.65$ among all the cases where we could demonstrate that merging occurs eventually. Conventions are as in Fig. 2.

In equation (5.1), the velocity is in units of $(GM_1/R_1)^{1/2}$, and we have taken $2G(M_1 + M_2)/(R_1 + R_2) \simeq v_{\rm esc,1}^2 = 2$. Various cross sections can be calculated:

1. The cross section $\sigma_{\rm col}$ for physical collision (encounters with $r_p \le R_1 + R_2$) is given by

$$\frac{\sigma_{\rm col}}{\pi(R_1 + R_2)^2} = 1 + \frac{2}{v_\infty^2} . \tag{5.2}$$

2. The cross section $\sigma_{\rm cap}$ for capture (i.e., formation of a bound system) is obtained by setting $r_p = r_{\rm cap}$ (see eq. [4.4]). Thus

$$\frac{\sigma_{\rm cap}}{\pi(R_1 + R_2)^2} = x_{\rm cap}^2 + x_{\rm cap}\frac{2}{v_\infty^2} , \tag{5.3a}$$

with

$$x_{\rm cap} \equiv \frac{r_{\rm cap}}{R_1 + R_1} = A_{\rm cap}\left(\frac{0.173}{v_\infty}\right)^\eta , \tag{5.3b}$$

where η is given in equation (4.4) and $A_{\rm cap}$ is given in Table 1, or, more approximately, by expression (4.5). In the limit of low velocity, $v_\infty \ll 1$, this cross section has the same scaling as that of tidal capture (Press & Teukolsky 1977; Lee & Ostriker 1986)

$$\frac{\sigma_{\rm cap}}{\pi(R_1 + R_2)^2} \simeq 1.46 q^{-0.1} v_\infty^{-2.18} , \quad \text{for} \quad v_\infty \ll 1 . \tag{5.4}$$

3. The merger cross section $\sigma_{\rm mrg}$ is obtained by setting $r_p = r_{\rm mrg}$ (cf. eq. [4.11]). Thus

$$\sigma_{\rm mrg} = \begin{cases} \sigma_{\rm col} , & \text{if} \quad v_\infty < v_{\rm mrg} ; \\ \sigma_{\rm cap} , & \text{if} \quad v_\infty \ge v_{\rm mrg} . \end{cases} \tag{5.5}$$

Here we have taken $C = 1$ in expression (4.11), and $v_{\rm mrg}$ is determined by setting $\sigma_{\rm col} = \sigma_{\rm cap}$.

4. The cross section for mass loss $\sigma_{\rm ml}$ is defined as in Benz & Hills (1987),

$$\sigma_{\rm ml} \equiv \int f_{\rm ml}(r_p) 2\pi b \, db$$

$$= \pi(R_1 + R_2)^2 \int_0^\infty f_{\rm ml}(x_p)\left(2x_p + \frac{2}{v_\infty^2}\right) dx_p . \tag{5.6}$$

The usefulness of this definition will become apparent in § 5.2. One can use the results shown in Figure 13 to calculate this cross section numerically. However, it is more convenient to use our fitting formula, expression (4.9). This gives

$$\frac{\sigma_{\rm ml}}{\pi(R_1+R_2)^2} \simeq f_{\rm ml}(r_p=0)x_{\rm ml}\left[x_{\rm ml}\left(1+\frac{\pi^2}{3}\frac{\Delta x_{\rm ml}^2}{x_{\rm ml}^2}\right)+\frac{2}{v_\infty^2}\right], \tag{5.7}$$

where we have used the identity

$$\int_0^\infty \frac{\psi(x)}{e^{x-\xi}+1}\,dx \simeq \int_0^\xi \psi(x)dx + \frac{\pi^2}{6}\left(\frac{d\psi}{dx}\right)_{x=\xi} \quad \text{for} \quad \xi \gg 1\,. \tag{5.8}$$

Notice from Table 1 that $\Delta x_{\rm ml}/x_{\rm ml} = \Delta A_{\rm ml}/A_{\rm ml} \sim 0.2$, so that equation (5.7) becomes

$$\frac{\sigma_{\rm ml}}{\pi(R_1+R_2)^2} \simeq f_{\rm ml}(r_p=0)x_{\rm ml}\left(1.1x_{\rm ml}+\frac{2}{v_\infty^2}\right). \tag{5.9}$$

In this expression, $f_{\rm ml}(r_p=0)$ is given by equation (4.7) together with Table 1 (or eq. [4.8]) and $x_{\rm ml}$ is given by equation (4.10) with parameters given in Table 1.

5.2. *Rates*

We now consider a star cluster containing different types of stars. The velocities of each type of stars is described by a Maxwell-Bolzmann distribution. The rate of a certain process (e.g., capture) between two types of stars (designated by subscripts 1 and 2) per unit volume can be written

$$\Gamma_p = \frac{n_1 n_2}{1+\delta_{12}}\langle\sigma_p v_\infty\rangle\,,$$

with

$$\langle\sigma_p v_\infty\rangle \equiv \int v_\infty\,\sigma_p(v_\infty)f(v_\infty)d^3v_\infty\,, \tag{5.10}$$

where n_i ($i=1, 2$) is the number density of stellar type i, and δ_{12} is unity if stellar type 1 and 2 are identical and zero otherwise. The distribution $f(v_\infty)$ of the relative velocity between stars of type 1 and 2 is also Maxwellian,

$$f(v_\infty) = \left(\frac{3}{2\pi}\right)^{3/2} v_{\rm rms}^{-3}\exp\left(-\frac{3v_\infty^2}{2v_{\rm rms}^2}\right), \tag{5.11}$$

where $v_{\rm rms}^2 = v_{{\rm rms},1}^2 + v_{{\rm rms},2}^2$ is the sum of the squares of the velocity dispersions for stellar types 1 and 2.

Using the results of § 5.1, we can now calculate rates for various processes between stellar types 1 and 2 by substituting the corresponding cross sections into equation (5.10). For convenience, we define a nondimensional rate Σ_p by

$$\Sigma_p \equiv \frac{\langle\sigma v_\infty\rangle_p}{\pi(R_1+R_2)^2 v_{\rm rms}}\,. \tag{5.12}$$

Using equations (5.2) and (5.10), we find that the collision rate is simply given by

$$\Sigma_{\rm col} = 4\left(\frac{3}{2\pi}\right)^{1/2}\left(\frac{1}{3}+\frac{1}{v_{\rm rms}^2}\right). \tag{5.13}$$

For other quantities, we evaluate expression (5.12) numerically. In Figure 16, the variation of Σ for collision, capture, merger and mass loss is shown as a function of velocity dispersion $v_{\rm rms}$ for two identical types of stars with $\alpha_1 = \alpha_2 = 10$ (To avoid the divergence near $v_{\rm rms} = 0$, we have actually plotted $v_{\rm rms}^2\,\Sigma$).

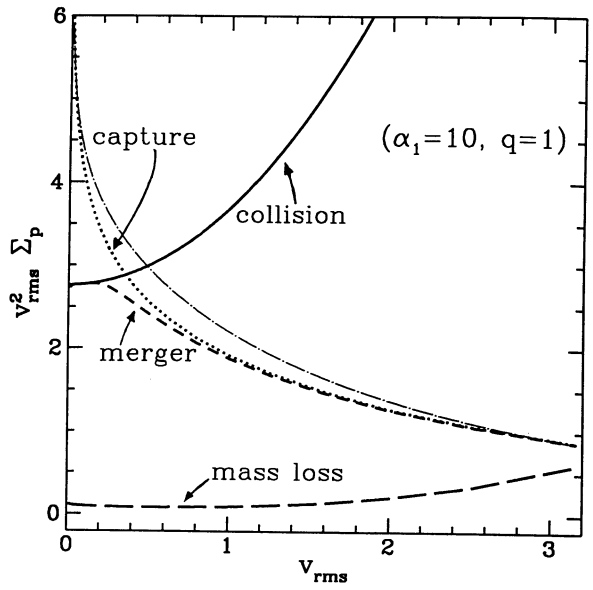

FIG. 16.—Nondimensional rate Σ_p (eq. [5.13]) for various processes is shown as a function of the relative velocity dispersion $v_{\rm rms}$ [in units of $(GM_1/R_1)^{1/2}$]. Results are shown for the case of $\alpha_1 = 10$ and $q = 1$. The solid line shows $\Sigma_{\rm col}$ for physical collision, the dotted line $\Sigma_{\rm cap}$ for capture, the dashed line $\Sigma_{\rm mrg}$ for merger, and the long-dashed line $\Sigma_{\rm ml}$ for mass loss. The dotted-dashed line shows our approximate analytic expression for $\Sigma_{\rm cap}$ (eq. [5.15]).

In the limit of $v_{\rm rms} \ll 1$, the nondimensional capture rate can be obtained analytically. We find

$$\Sigma_{\rm cap} \simeq 2.19 A_{\rm cap} v_{\rm rms}^{-2.18}\,, \tag{5.14a}$$

with

$$A_{\rm cap} \simeq \frac{1}{q^{0.1}}\,, \quad \text{for} \quad v_{\rm rms} \ll 1\,. \tag{5.14b}$$

Expression (5.14) gives the tidal capture rate, and it is close to the result from linear perturbation theory (see § 4.2). For arbitrary $v_{\rm rms}$, we can also obtain an approximate analytic expression for $\Sigma_{\rm cap}$,

$$\Sigma_{\rm cap} \simeq 2.19 q^{-0.1} v_{\rm rms}^{-2-\eta'}\,, \tag{5.15a}$$

with

$$\eta' = 0.18 + \left(\frac{v_{\rm rms}}{8}\right)^{1/2}. \tag{5.15b}$$

Expression (5.15) reduces to expression (5.14) in the limit of $v_{\rm rms} \ll 1$. In Figure 16, expression (5.15) is shown together with the more accurate numerical results. We see that there is good agreement, to within about 20% for all $v_{\rm rms}$. The stellar capture rate is therefore given approximately by

$$\Gamma_{\rm cap} = \frac{n_1 n_2}{1+\delta_{12}}\pi(R_1+R_2)^2 v_{\rm rms}\,\Sigma_{\rm cap}$$

$$\simeq \frac{n_1 n_2}{1+\delta_{12}} \times 2.19\pi(R_1+R_2)^2 q^{-0.1} v_{\rm rms}^{-1-\eta'}\,. \tag{5.16}$$

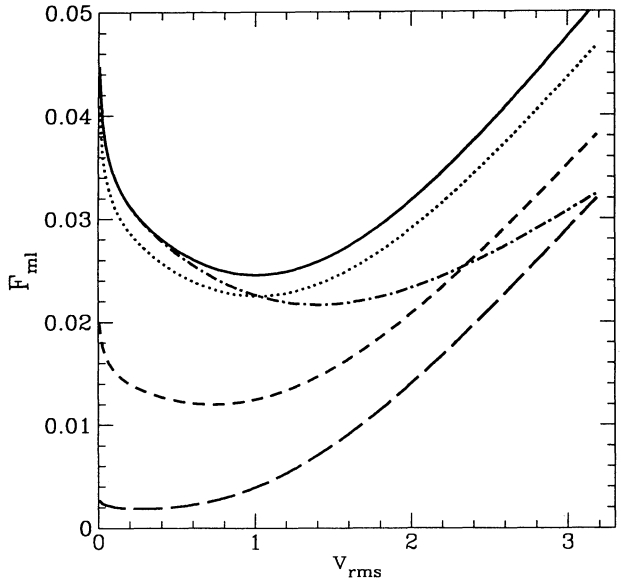

FIG. 17.—Average fractional mass loss per collision F_{ml} (defined in eq. [5.18]) as a function of relative velocity dispersion v_{rms} [in units of $(GM_1/R_1)^{1/2}$] for different mass combinations. The solid line is for $\alpha_1 = 10$, $q = 1$, the dotted line for $\alpha_1 = 10$, $q = 0.5$, the short-dashed line for $\alpha_1 = 10$, $q = 0.2$, the long-dashed line for $\alpha_1 = 10$, $q = 0.1$, and the dotted-dashed line for $\alpha_1 = 1$ and $q = 1$.

For equal-mass solar-type MS stars, expression (5.16) gives

$$\Gamma_{cap} \simeq 3 \times 10^{-5} \left(\frac{n}{10^6 \text{ pc}^{-3}}\right)^2 \left(\frac{R}{R_\odot}\right)^2 \times \left(\frac{v_{rms}}{100 \text{ km s}^{-1}}\right)^{-1.35} \text{pc}^{-3} \text{ yr}^{-1}, \quad (5.17)$$

where we have evaluated η' for $v_{rms} = 100$ km s^{-1}.

The merger rate can be obtained similarly. In Figure 16, we see that for high velocity dispersion ($v_{rms} \gtrsim 0.3$), it is nearly identical to the capture rate, while for low velocity dispersion, it is approximately equal to the collision rate (Recall that we have set $C = 1$ in eq. [4.11]). The turn-over is around $v_{rms} \simeq 0.3$.

The average fractional mass-loss rate per unit volume, due to collisions between stars of type 1 and type 2, Γ_{ml}, can be calculated using equation (5.10) together with expression (5.9) for the mass-loss cross section. However, it is more convenient to define F_{ml}, the *average fractional mass loss per collision* between stellar types 1 and 2, by

$$F_{ml} \equiv \frac{\Gamma_{ml}}{\Gamma_{col}} = \frac{\Sigma_{ml}}{\Sigma_{col}} \simeq \frac{9}{2v_{rms}^2(v_{rms}^2 + 3)} \int_0^\infty f_{ml}(r_p = 0) x_{ml} \times \left(1.1 x_{ml} + \frac{2}{v_\infty^2}\right) v_\infty^2 \exp\left(-\frac{3v_\infty^2}{2v_{rms}^2}\right) dv_\infty . \quad (5.18)$$

The variation of F_{ml} as a function of v_{rms} is plotted in Figure 17 for different mass combinations. Notice that F_{ml} does not increase monotonically as v_{rms} increases. In the limit of $v_{rms} \ll 1$, more encounters result in a mass-loss fraction comparable to that in a head-on collision, $f_{ml}(r_p = 0)$, i.e., $x_{ml} \propto v_\infty^{-0.1}$ increases as v_∞ decreases (see eq. [4.10]). On the other hand, in this limit, $f_{ml}(r_p = 0)$ is nearly independent of v_∞, with

$$f_{ml}(r_p = 0) \simeq f_{ml}(r_p = 0, v_\infty = 0) = C_{ml}$$

(see eq. [4.7]). Therefore, the value of F_{ml} in this regime is mainly determined by the mass-loss fraction in a head-on collision, and $F_{ml} \propto v_{rms}^{-0.1}$ decreases as v_{rms} increases. In the opposite limit $v_{rms} \gg 1$, the dominant factor is the rapid increase in $f_{ml}(r_p = 0) \propto v_\infty^{2.8}$, causing F_{ml} to increase with v_{rms}. However, since the proportion of encounters leading to negligible mass loss increases as v_∞ increases (i.e., x_{ml} decreases), the value of F_{ml} must increase more slowly than $f_{ml}(r_p = 0)$. From equations (4.7), (4.10), and (5.18), we find that, approximately, $F_{ml} \propto v_{rms}^{2.8 - 2\delta'}$, where $\delta' \simeq 0.1(1 + v_{rms}^{1/2})$. For $1 \lesssim v_{rms} \lesssim 3$, we expect F_{ml} to increase much more slowly than $f_{ml}(r_p = 0)$. In fact, Figure 17 shows that *the average mass loss fraction per collision remains very small.* For example, for collisions between two identical stars with $\alpha = 10$, F_{ml} varies from about 2% to 5% for velocity dispersion $0 < v_{rms} < 3$. In contrast, for a single head-on collision (Fig. 12), the mass loss fraction f_{ml} varies from about 6% to 50% for $0 < v_\infty < 3$.

6. SUMMARY

We have studied numerically the physics of collisions and close encounters between massive MS stars ($1 M_\odot \lesssim M \lesssim 100 M_\odot$) represented by Eddington standard models. We have found that a variety of qualitatively different outcomes are possible depending on the orbital parameters of the encounter as well as the masses of the two stars. We have tried to present our numerical results in a simple, convenient form. For individual encounters, our main quantitative results are as follows:

1. For given impact velocity and given stellar types, the capture radius r_{cap} is given approximately by equations (4.4) and (4.5), together with Table 1. For small relative velocity, tidal dissipation dominates, and r_{cap} is close to the value determined from linear perturbation theory (e.g., Lee & Ostriker 1986). However, our result for r_{cap} is about 10% higher, indicating that linear theory underestimates the tidal dissipation. For high relative velocity [$v_\infty \gtrsim 0.2(GM/R)^{1/2}$], shock dissipation dominates and the critical capture radius r_{cap} decreases faster than predicted by linear theory as v_∞ increases.

2. The fractional mass loss in a stellar collision is given approximately by equation (4.7) or (4.8) for head-on collisions, and by equations (4.9) and (4.10) for off-axis collisions. These fitting formulae, quoted for arbitrary velocity and impact parameter, provide a reasonable estimate of the mass-loss fraction in any collision, with an overall accuracy of about 30%.

3. All dissipative encounters leading to capture after the first periastron passage are likely to result eventually in a merger. The critical periastron distance for merger is given approximately by equation (4.11). Our results indicate that the merger rate is somewhat higher than estimated in previous work.

We have determined the cross sections and rates for various processes occurring in star clusters (eqs. [5.13]–[5.17]). The average mass-loss per collision (eq. [5.18] and Fig. 17) does not depend sensitively on the velocity dispersion of the cluster, although for an individual head-on collision, the mass losses increase rapidly with impact velocity. Our results indicate that even for a star cluster with a velocity dispersion as high as several times the typical escape velocity from a MS star ($\simeq 600$ km s^{-1}), stellar collisions are not very disruptive on average. This is in contrast to what has been assumed in several studies

of galactic nuclei. Thus a reevaluation of the role played by stellar collisions in these systems seems desirable.

We thank R. Durisen, B. Murphy, E. Salpeter, and S. Teukolsky for useful discussions. This work has been supported in part by NSF grant AST 91-19475 and NASA grant NAGW-2364 to Cornell University. Partial support was also provided by NASA through grant HF-1037.01-92A awarded by the Space Telescope Science Institute which is operated by the Association of Universities for Research in Astronomy, Inc., for NASA under contract NAS5-26555. Computations were performed at the Cornel National Supercomputer Facility, a resource of the Center for Theory and Simulation in Science and Engineering at Cornell University, which receives major funding from the NSF and from the IBM Corporation, with additional support from New York State and members of its Corporate Research Institute.

REFERENCES

Bahcall, J. N., & Wolf, R. A. 1976, ApJ, 209, 214
Begelman, M. C., & Rees, M. J. 1978, MNRAS, 185, 847
Benz, W., & Hills, J. G. 1987, ApJ, 323, 614
———. 1992, ApJ, 389, 546
Binney, J., & Tremaine, S. 1987, Galactic Dynamics (Princeton: Princeton Univ. Press)
Carter, B., & Luminet, J.-P. 1985, MNRAS, 212, 23
Clayton, D. D. 1983, Principles of Stellar Evolution and Nucleosynthesis (Chicago: Univ. Chicago Press)
Cleary, P. W., & Monaghan, J. J. 1990, ApJ, 349, 150
Colgate, S. A. 1967, ApJ, 150, 163
David, L. P., Durisen, R. H., & Cohn, H. N. 1987a, ApJ, 313, 556
———. 1987b, ApJ, 316, 505
Davies, M. B., Benz, W., & Hills, J. G. 1992, ApJ, 401, 246
DeYoung, D. S. 1968, ApJ, 153, 633
Di Stefano, R., & Rappaport, S. 1992, ApJ, 396, 587
Dressler, A. 1989, in Active Galactic Nuclei, ed. D. E. Osterbrock & J. S. Miller (Dordrecht: Kluwer), 217
Dressler, A., & Richstone, D. O. 1988, ApJ, 324, 701
Fabian, A. C., Pringle, J. E., & Rees, M. J. 1975, MNRAS, 172, 15P
Frank, J., & Rees, M. J. 1976, MNRAS, 176, 633
Gingold, R. A., & Monaghan, J. J. 1977, MNRAS, 181, 375
Gold, T., Axford, W. I., & Ray, E. C. 1965, in Quasi-Stellar Sources and Gravitational Collapse, ed. I. Robinson et al. (Chicago: Univ. Chicago Press), 93
Goodman, J., & Hernquist, L. 1991, ApJ, 378, 637
Guhatakurta, P., Yanny, B., Schneider, D., & Bahcall, J. N. 1993, in Proc. of STScI Workshop on Blue Stragglers, ed. M. Livio & R. Saffer (ASP Conf. Ser.), in press
Hernquist, L., & Katz, N. 1989, ApJS, 70, 419
Hills, J. G., & Day, C. A. 1976, Astrophys. Lett., 17, 87
Hut, P., et al. 1992, PASP, 104, 981
Kochanek, C. S. 1992, ApJ, 385, 604
Kormendy, J. 1988, ApJ, 325, 128
———. 1993, in The Nearest Active Galaxies, ed. J. E. Beckman, H. Netzer, & L. Colina, in press
Kosovichev, A. G., & Novikov, I. D. 1992, MNRAS, 258, 715
Lauer, T. R., et al. 1992, AJ, 103, 703
———. 1993, AJ, in press
Lee, H. M., & Ostriker, J. P. 1986, ApJ, 310, 176
Leonard, P. J. T. 1989, AJ, 98, 217
Lightman, A. P., & Shapiro, S. L. 1976, 211, 244
Lucy, L. B. 1977, AJ, 82, 1013
McMillan, S. L. W., McDermott, P. N., & Taam, R. E. 1987, ApJ, 318, 261
Mathis, J. 1967, ApJ, 147, 1050
Meylan, G. 1993, in Dynamics of Globular Clusters: a Workshop in Honor of Ivan R. King, ed. S. Djorgovski & G. Meylan (ASP Conf. Ser.), in press
Monaghan, J. J. 1992, ARA&A, 30, 543
Murphy, B. W., Cohn, H. N., & Durisen, R. H. 1991, ApJ, 370, 60
Paresce, F., et al. 1991, Nature, 352, 297
———. 1993, in Proc. of STScI Workshop on Blue Stragglers, ed. M. Livio & R. Saffer (ASP Conf. Ser.), in press
Pols, O. 1993, Proc. of STScI Workshop on Blue Stragglers, ed. M. Livio & R. Saffer (ASP Conf. Ser.), in press
Press, W. H., & Teukolsky, S. L. 1977, ApJ, 213, 183
Quinlan, G. D., & Shapiro, S. L. 1989, ApJ, 343, 725
———. 1990, ApJ, 356, 483
Ray, A., Kembhavi, A. K., & Antia, H. M. 1987, A&A, 184, 164
Rasio, F. A., & Shapiro, S. L. 1991, ApJ, 377, 559
———. 1992, ApJ, 401, 226
Rees, M. J. 1984, ARA&A, 22, 471
———. 1990, Science, 247, 817
Różyczka, M., Yorke, H. W., Bodenheimer, P., Müller, E., & Hashimoto, M. 1989, A&A, 208, 69
Ruffert, M. 1992, MPI preprint
Ruffert, M., & Müller, E. 1990, A&A, 238, 116
Sanders, R. H. 1970, ApJ, 162, 791
Sarajedini, A. 1993, in Proc. of STScI Workshop on Blue Stragglers, ed. M. Livio & R. Saffer (ASP Conf. Ser.), in press
Seidl, F. G. P., & Cameron, A. G. W. 1972, Ap&SS, 15, 44
Shapiro, S. L. 1985, in Dynamics of Star Clusters, ed. J. Goodman & P. Hut (Dordrecht: Reidel)
Shapiro, S. L., & Teukolsky, S. A. 1985, ApJ, 292, L41
Spitzer, L. 1987, Dynamical Evolution of Globular Clusters (Princeton: Princeton Univ. Press)
Spitzer, L., & Saslaw, W. C. 1966, ApJ, 143, 400
Spitzer, L., & Stone, M. E. 1967, ApJ, 147, 519
Steinmetz, M., & Müller, E. 1993, A&A, submitted
Tassoul, J.-L. 1978, Theory of Rotating Stars (Princeton: Princeton Univ. Press)
Zel'dovich, Y. B., & Podurets, M. A. 1965, Soviet Astron., 9, 742